Supporting Information

for

Metal-ligand bonding in tricarbonyliron(0) complexes bearing thiochalcone ligands

by

Piotr Matczak,[1] Stephan Kupfer,[2] Grzegorz Mlostoń,[3] Philipp Buday,[4] Helmar Görls,[4] Wolfgang Weigand[4]

[1] Department of Physical Chemistry, Faculty of Chemistry, University of Lodz, Pomorska 163/165, 90236 Lodz, Poland

[2] Institute of Physical Chemistry, Friedrich Schiller University Jena, Helmholtzweg 4, 07743 Jena, Germany

[3] Department of Organic and Applied Chemistry, Faculty of Chemistry, University of Lodz, Tamka 12, 91403 Lodz, Poland

[4] Institute of Inorganic and Analytical Chemistry, Friedrich Schiller University Jena, Humboldtstrasse 8, 07743 Jena, Germany

Section S1. Crystal structure determination

The crystal structure of complexes **2** and **5** was determined by its single-crystal XRD analysis. The intensity data for these complexes were collected on a Nonius KappaCCD diffractometer using graphite-monochromated Mo-K_α radiation. Data were corrected for Lorentz and polarization effects; absorption was taken into account on a semi-empirical basis using multiple-scans.[1-3]

The structures were solved by direct methods (SHELXS)[4] and refined by full-matrix least squares techniques against Fo^2 (SHELXL-2018).[5] The hydrogen atoms of compounds **5** with exception of the disordered 2-furyl group were located by difference Fourier synthesis and refined isotropically. All other hydrogen atoms were included at calculated positions with fixed thermal parameters. All non-hydrogen atoms were refined anisotropically.[5]

Disordered 2-thienyl and 2-furyl groups were refined using bond lengths restraints and displacement parameter restraints. Some parts of the disorder model were introduced by the program DSR.[6] XP was used for structure representations.[7] The molecular structures of complexes **2** and **5** in their crystals are shown in Figures S1 and 1, respectively.

Crystal data for complex **2**: $C_{16}H_{10}FeO_3S_2$, Mr = 370.21 $gmol^{-1}$, brown prism, size 0.088 x 0.082 x 0.044 mm^3, triclinic, space group P ī, a = 6.4288(4), b = 8.8456(5), c = 14.0419(9) Å, α = 105.769(3), β = 99.980(3), γ = 99.222(3)°, V = 738.50(8) $Å^3$, T = -140 °C, Z = 2, $\rho_{calcd.}$ = 1.665 gcm^{-3}, μ (Mo-K_α) = 13.11 cm^{-1}, multi-scan, transmin: 0.6271, transmax: 0.7456, F(000) = 376, 6988 reflections in h(-8/5), k(-11/11), l(-18/18), measured in the range 2.452° ≤ Θ ≤ 27.483°, completeness Θ_{max} = 99.1%, 3352 independent reflections, R_{int} = 0.0441, 2635 reflections with $F_o > 4\sigma(F_o)$, 215 parameters, 144 restraints, $R1_{obs}$ = 0.0878, wR^2_{obs} = 0.2155,

$R1_{all}$ = 0.1115, wR^2_{all} = 0.2348, GOOF = 1.094, largest difference peak and hole: 2.215/-0.639 e Å^{-3}.

Crystal data for complex **5**: $C_{20}H_{14}Fe_2O_4S$, Mr = 462.07 gmol^{-1}, red-brown prism, size 0.098 x 0.082 x 0.078 mm^3, monoclinic, space group P 2_1, a = 7.1138(5), b = 19.2710(9), c = 7.4050(5) Å, β = 117.245(3)°, V = 902.53(10) Å^3 , T = -140 °C, Z = 2, $\rho_{calcd.}$ = 1.700 gcm^{-3}, μ (Mo-K_α) = 17.46 cm^{-1}, multi-scan, transmin: 0.6970, transmax: 0.7456, F(000) = 468, 7032 reflections in h(-9/8), k(-25/24), l(-9/9), measured in the range 2.114° ≤ Θ ≤ 27.470°, completeness Θ_{max} = 99.9%, 4039 independent reflections, R_{int} = 0.0238, 3951 reflections with $F_o > 4\sigma(F_o)$, 301 parameters, 77 restraints, $R1_{obs}$ = 0.0233, wR^2_{obs} = 0.0499, $R1_{all}$ = 0.0242, wR^2_{all} = 0.0507, GOOF = 1.052, Flack-parameter 0.028(10), largest difference peak and hole: 0.244/-0.246 e Å^{-3}.

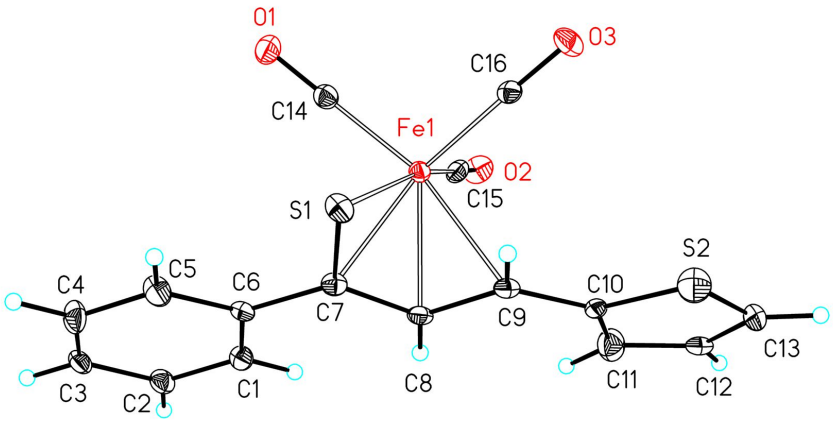

Figure S1. Molecular structure of complex **2**. The ellipsoids represent a probability of 30%, H atoms are shown with arbitrary radii.

It should be noted that some difficulties with crystal structure determination were encountered for complex **2**. In consequence, the R values presented above for the crystal structure of complex **2** are high and other descriptors shown in Figure S2 also indicate the presence of certain errors affecting the quality of this structure. Additional efforts were made to determine the crystal structure of complex **2** as accurately as possible. Data collection was carried out with different crystals, crystals from different crystallisation approaches and different batches with an optimised measurement strategy were used. The absorption correction was varied. An attempt was also made to treat the data reduction as a twin. The data reduction was repeated with the current version of BRUKER software. However, the same problems occurred in all attempts. These included the peaks in the electron density, which cannot be interpreted chemically, and therefore they are considered as artefacts, with different causes (crystal quality, truncation effects in Fourier synthesis, absorption effects etc.) The problem of the disorder of the 2-thienyl group could only be treated by numerous use of restraints/constraints and the use of the 2-thienyl fragment from the DSR program. To conclude, a number of attempts were made to improve the crystal structure of complex **2**, but they all led to the same structure as that reported above.

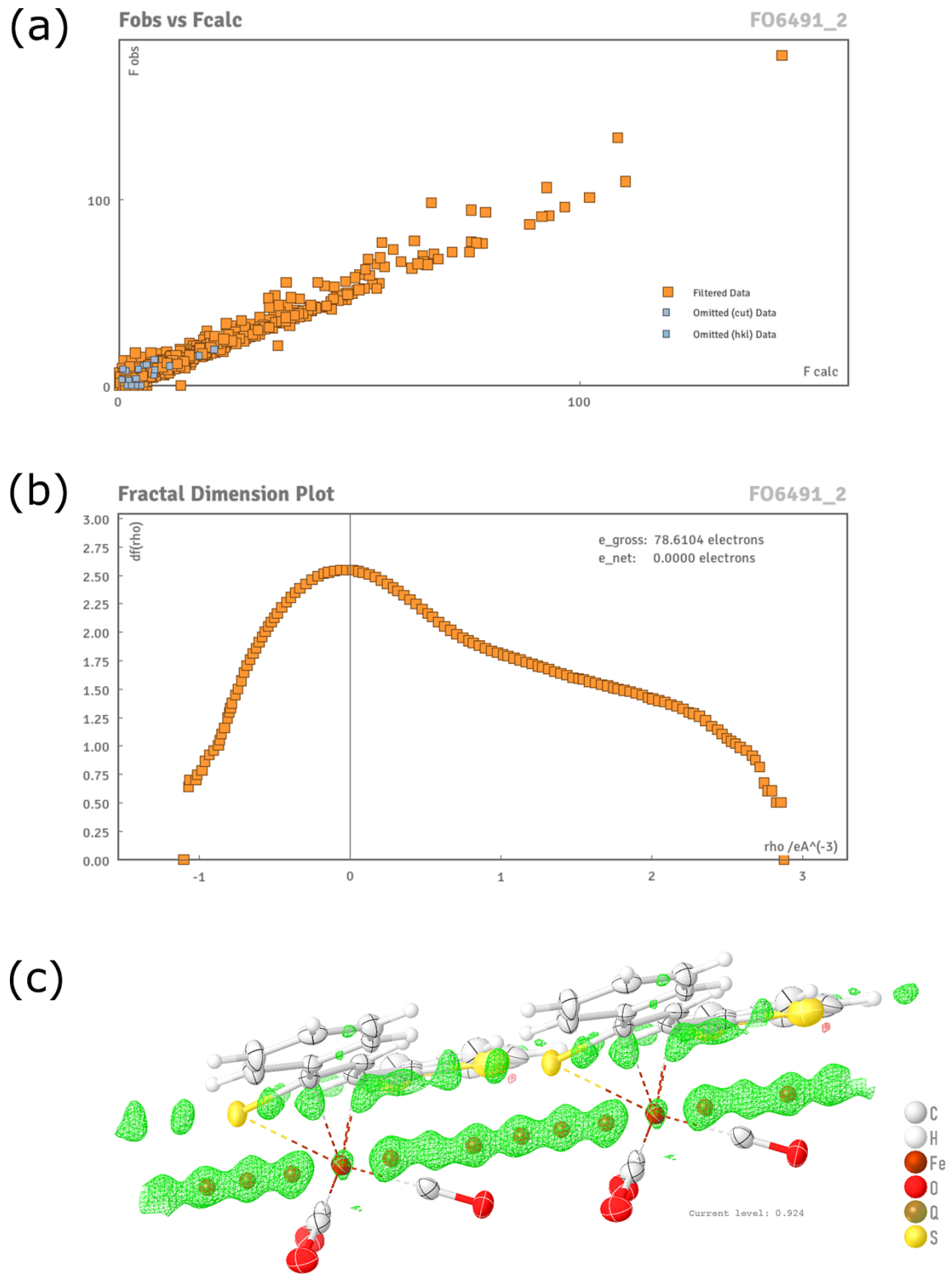

Figure S2. Plots of (a) the residual density, (b) the fractal dimension distribution of the residual density and (c) the crystal structure with visible artefacts for complex **2**, as determined by its single-crystal XRD analysis.

Section S2. Further computational details

The choice of the ωB97X-D density functional for the geometry optimization of **1**–**7** was verified by comparison with the performance of two other popular density functionals in reproducing the experimental metal-ligand interatomic distances in complexes **1**–**6**. The experimental metal-ligand interatomic distances were taken from Section S1 (**2** and **5**) and our previous study in which the XRD crystal structures of **1, 3, 4** and **6** were measured. The M06-2X and B3LYP functionals were selected as other popular density functionals used for studying organometallic compounds. The isolated complexes of **1**–**6** in their initial geometries extracted from the corresponding XRD crystal structures were taken for geometry optimization at the ωB97X-D/def2-SVP, M06-2X/def2-SVP and B3LYP/def2-SVP levels of theory. For the complexes in their optimized geometries at a given level of theory, their metal-ligand interatomic distances were compared with the experimental results in a statistical manner. The values of the mean unsigned error (MUE) between the calculated and experimental metal-ligand interatomic distances for **1**–**6** are shown in Table S1. From these MUE values, it can be concluded that the ωB97X-D/def2-SVP level reproduces the experimental metal-ligand distances most accurately.

Table S1. Mean unsigned errors for the geometrical structures of **1**–**6** optimized using different density functionals.

Level of theory	MUE (in pm)
ωB97X-D/def2-SVP	1.81
M06-2X/def2-SVP	5.48
B3LYP/def2-SVP	1.93

The geometries of both complexes **1**–**7** and their isolated thiadiene ligands were optimized at the ωB97X-D/def2-SVP level of theory. Harmonic vibrational frequency calculations for the complexes and the free thiadienes were performed at the same level of

theory to verify that the optimized structures corresponded to true local minima on the 3*N*-6 dimensional potential energy surface. The ωB97X-D/def2-SVP wave functions of **1**–**7** in their optimized geometries were evaluated to ensure that no instabilities occurred.

For **1**–**6**, their three spin states, that is, singlet, triplet and quintet, were considered in the geometry optimizations. The singlet spin state could actually be expected to be the ground state of **1**–**6** because 18-electron complexes of iron are often singlet species,[8] as it is observed for 18-electron $Fe(CO)_5$.[9] On the other hand, the triplet ground state of $Fe(CO)_3$ in rare-gas matrices was previously deduced from experimental observations[10,11] and theoretical calculations,[12,13] and therefore we also optimized the geometries of **1**–**6** in their triplet state. The quintet spin state was additionally inspected to ensure that high-spin configurations make the η^4-coordination of 1-thia-1,3-diene unlikely. The considered spin states of **1**–**6** are connected to the specific occupancies of valence orbitals in $Fe(CO)_3$ and to the splitting of the d-orbitals of Fe. Chart S1 shows three valence electron configurations for $Fe(CO)_3$ in its pyramidal C_{3v} geometry. The ordering of energy levels was taken from the classical paper by Elian and Hoffmann.[14] The Fe atom in $Fe(CO)_3$ is best approximated as featuring a d^8 configuration (due to the occupation of the 3d shell by two 4s electrons). Then, two lower e levels are primarily metal-centered $3d_{xy}$ and $3d_{x^2-y^2}$ orbitals, the lower a_1 level is $3d_{z^2}$, and two higher e levels are predominantly of $3d_{xz}$ and $3d_{yz}$ character;[14] all these assignments obviously depend on the coordinate system chosen. The higher a_1 level is a sp-hybrid orbital. For the sake of simplicity, we omit to discuss the possibility for the removal of e-level degeneracy as a result of Jahn-Teller effects for the singlet spin state in Chart S1.

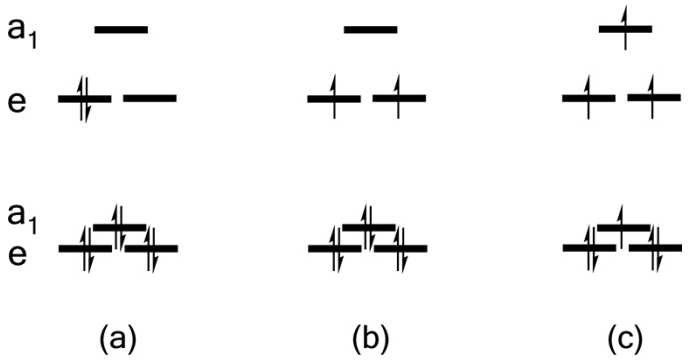

Chart S1. Schematic representation of valence energy levels and orbital occupancies of $Fe(CO)_3$ in its (a) singlet, (b) triplet, and (c) quintet spin states.

The geometry optimizations of **1**–**6** in all three spin states were carried using the ωB97X-D functional based on unrestricted determinants (commonly denoted by UωB97X-D). The $\langle \mathbf{S}^2 \rangle$ values obtained from these UωB97X-D/def2-SVP calculations were very close to the corresponding $S_z(S_z + 1)$ values. Thus, the UωB97X-D/def2-SVP results did not suffer significantly from "spin contamination" although we are aware that this concept is not well defined in DFT methods. The geometry optimizations of **1**–**6** in the closed-shell singlet electronic configuration were additionally carried using the ωB97X-D functional with the respective restricted-type determinant (commonly denoted by RωB97X-D). The RωB97X-D/def2-SVP results were identical to those obtained from UωB97X-D/def2-SVP for the singlet spin state; some marginal differences in energies ($< 10^{-7}$ a.u.) could be observed but they were completely irrelevant to the geometries of **1**–**6** and the analysis of their metal-ligand bonding properties.

The predicted ground state of **1**–**6** is of closed-shell singlet nature that can be related to the assumed electronic configurations of $Fe(CO)_3$ and of the thiochalcone fragments. Figure S3 presents the orbital diagram of complex **1** as well as of its $Fe(CO)_3$ and thiochalcone fragments; all calculated at the ωB97X-D/def2-SVP level of theory. In this figure, the energy levels and orbitals contours of $Fe(CO)_3$ and thiochalcone were determined for these molecular

fragments in their geometries taken from the fully relaxed complex (in consequence, the $Fe(CO)_3$ fragment adopted a distorted pyramidal structure). The diagram illustrates an electron transfer from the HOMO of thiochalcone to the LUMO of $Fe(CO)_3$. There is also a reverse transfer from the HOMO of $Fe(CO)_3$ to the LUMO of thiochalcone. These charge transfer properties indicate the occurrence of metal←ligand donation and synergistic metal→ligand back-donation in **1**–**6**. It should be noted that the orbital mixing marked in Figure S3 is a simplification: the symmetry of the complex is low and a mix of the respective orbitals is not forbidden by means of symmetry.

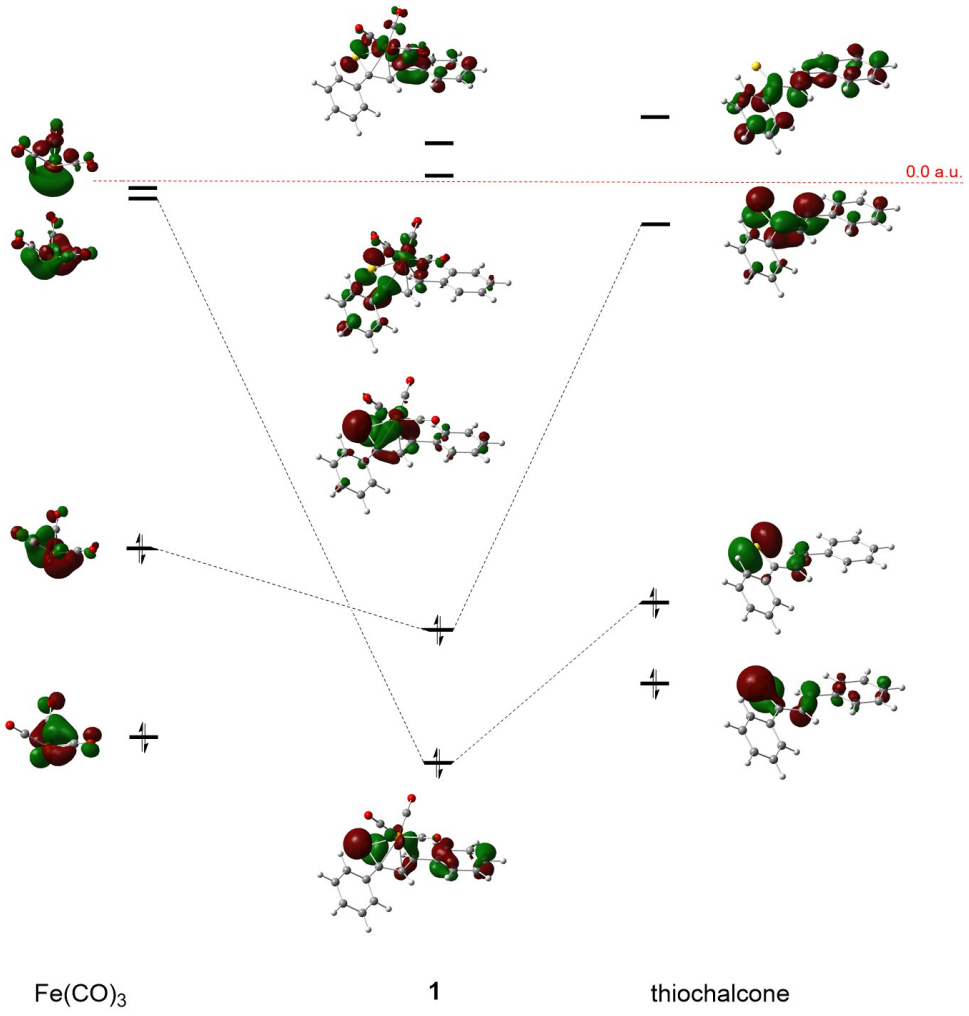

Figure S3. Diagram of the frontier molecular orbitals for singlet ground-state complex **1** and its $Fe(CO)_3$ and thiochalcone fragments. The orbital contours are plotted with an isovalue of 0.05 a.u.

The distribution of electron charge among the metal center and ligands of **1**–**7** was probed using the QTAIM partial atomic charges of the Fe center and the atoms constituting the carbonyl and thiadiene ligands. The partial atomic charges derived from the QTAIM method were previously recognized as a reliable descriptor of the charge distribution in transition metal carbonyl complexes.[15] By contrast, the atomic partial charges of the NBO method were not capable of providing a faithful description of the charge distribution in transition metal carbonyl complexes.

For each complex optimized at the ωB97X-D/def2-SVP level of theory, the binding energy (E_{bind}) between its $Fe(CO)_3$ and thiadiene fragments was computed in a supermolecular fashion at the MP2/def2-TZVPD level of theory. The E_{bind} energy was calculated as the difference between the total energy (E_{tot}) of the whole complex and the sum of the total energies of the $Fe(CO)_3$ and thiadiene fragments in their geometries taken from the complex.

$$E_{bind} = E_{tot}(\text{complex}) - [E_{tot}(Fe(CO)_3) + E_{tot}(\text{thiadiene})] \quad \text{(S1)}$$

The counterpoise correction proposed by Boys and Bernardi[16] was employed to assess and to correct the impact of the basis-set superposition error with respect to E_{bind}. Core electrons were excluded from the correlation treatment in the MP2 calculations.

The E_{bind} energy expresses the total interaction between the $Fe(CO)_3$ and thiadiene fragments in their complex. The negative value of E_{bind} indicates an attractive interaction between the fragments, and therefore this interaction stabilizes the complex.

IQA calculations were carried out using the B3LYP/def2-TZVPD wave functions of complexes **1**–**7** in their ωB97X-D/def2-SVP-optimized geometries. The reason behind the choice of the B3LYP density functional for the generation of wave functions was the

availability of true exchange electronic energies for this functional in the AIMAll implementation of the IQA method. It should be stressed that very few density functionals have been implemented in the IQA module of the AIMAll software so far.

Within the IQA method, the E_{bind} energy is retrieved from three contributions: the electronic deformation (E_{def}) suffered by fragments upon their complexation, the classical Coulombic interaction (E_{cl}) between fragments and their exchange-correlation interaction (E_{xc}).

$$E_{bind} = E_{def} + E_{cl} + E_{xc} \quad \text{(S2)}$$

Thus, the binding of fragments is the results of a competition between the destabilizing E_{def} contribution and the stabilizing E_{cl} and E_{xc} contributions. The E_{cl} contribution is associated with electrostatic interactions between fragments, while E_{xc} is the covalent-like interaction energy.

According to the IQA method, the E_{tot} energy of each complex was expressed as a sum of atomic self-energies (i.e., intra-atomic energies, E_{self}) and pairwise interatomic energies (E_{inter}):

$$E_{tot}(\text{complex}) = \sum_{A} E_{self}^{A} + \sum_{A>B} E_{inter}^{AB} \quad \text{(S3)}$$

In this equation E_{self}^{A} denotes the self-energy of atomic basin A (that is, atom A) and it includes all kinetic (T) and potential (V) energy terms that depend only on nucleus (n) and electrons (e) contained in atom A. The self-energy represents the energy released in building an atom from isolated electrons and the nucleus, being initially in their infinite separation. E_{inter}^{AB} collects all potential energy terms for interactions between two atomic basins A and B.

$$E_{\text{self}}^{\text{A}} = T^{\text{A}} + V_{\text{en}}^{\text{AA}} + V_{\text{ee}}^{\text{AA}} \tag{S4}$$

$$E_{\text{inter}}^{\text{AB}} = V_{\text{nn}}^{\text{AB}} + V_{\text{ne}}^{\text{AB}} + V_{\text{en}}^{\text{AB}} + V_{\text{C}}^{\text{AB}} + V_{\text{X}}^{\text{AB}} + V_{\text{corr}}^{\text{AB}} \tag{S5}$$

The last three terms on the right-hand side of Eq. (S5) denote the Coulomb, exchange and correlation interaction energy terms. All classical interaction terms in Eq. (S5) are usually grouped into a single contribution (V_{cl}), while all non-classical (i.e., quantum-mechanical) interaction terms are gathered together as V_{xc}.

$$V_{\text{cl}} = V_{\text{nn}}^{\text{AB}} + V_{\text{ne}}^{\text{AB}} + V_{\text{en}}^{\text{AB}} + V_{\text{C}}^{\text{AB}} \tag{S6}$$

$$V_{\text{xc}} = V_{\text{X}}^{\text{AB}} + V_{\text{corr}}^{\text{AB}} \tag{S7}$$

In the subsection “Orbital perspective”, the frontier molecular orbitals of the free thiadienes in their optimized geometries were plotted using their *ω*B97X-D/def2-SVP wave functions.

ETS-NOCV calculations were carried out using the *ω*B97X-D/def2-SVP wave functions of complexes **1**–**7** in their *ω*B97X-D/def2-SVP-optimized geometries. Instead of def2-TZVPD, the smaller basis set was used for these calculations because of the well-known issues with extended basis sets augmented by diffuse functions in the ETS-NOCV module of the Multiwfn program. The *ω*B97X-D/def2-SVP wave functions of complexes **1**–**7** were also used in NBO calculations. The def2-SVP basis set was chosen to avoid a possible issue with basis set linear dependence.

Section S3. Further results of NBO calculations

Natural bond orbital (NBO) calculations were carried out for the complexes **1**–**7**. The results of the calculations designate the bonding pattern shown in Chart 2 as the optimal Lewis-like structure for **1**–**7**. This structure shows the formation of two σ-type NBOs corresponding to the Fe-S and Fe-C^3 bonds. Simultaneously, the S-C^1 and C^2-C^3 bonds of the thiadienes reduce their double-bond character, while C^1-C^2 manifests the double-bond character. This bonding pattern satisfies the 12-electron configuration of the metal center ("duodectet rule") used in the NBO calculations.[17] An additional ω-bonding interaction (not shown in Chart 2) appears for C^3, Fe and one of carbonyl carbons (strictly speaking, the carbonyl C atom lying approximately on the extension of the Fe-C^3 bond and not forming a σ-type NBO with Fe in Chart 2). The ω-bonding is described as "three-center, four-electron (3c/4e) hypervalency."[17] For the optimal Lewis-like structures of **1**–**7**, delocalization effects were estimated by donor-acceptor orbital stabilization energies ($E^{(2)}$) derived from the NBO second-order perturbation theory.[17] Within the perturbation theory of donor-acceptor NBO interactions, the $E^{(2)}$ energy is associated with an electron delocalization between donor (Lewis-type) and acceptor (non-Lewis-type) NBOs of a parent Lewis-like structure. The calculated $E^{(2)}$ values of the leading donor-acceptor NBO interactions involving the metal center and the thiadiene ligands of **1**–**7** are listed in Table S2. It is evident that the delocalizations between the π/π^*-type NBOs of C^1-C^2 and the NBOs of Fe-S and Fe-C^3 produce a significant stabilizing effect. The formation of the Fe-S and Fe-C^3 NBOs could be viewed as a result of metal←ligand σ-donation during complexation (the contributions of Fe natural hybrid orbitals in the Fe-S and Fe-C^3 NBOs are smaller than those of S and C^3). Then, metal→ligand π-back-donation could be ascribed to the Fe→C^1-C^2 delocalization occurring from the lone pair orbitals of the metal center to the π^*-type NBOs of C^1-C^2. The Fe→C^1-C^2 delocalization leads to the $E^{(2)}$ energy that is less

stabilizing than the delocalizations involving the Fe-S, Fe-C^3 and C^1-C^2 NBOs. Thus, the dominant π-back-donation interaction predicted by the ETS-NOCV method cannot be claimed in an unambiguous fashion within the framework of the NBO method. On the other hand, the NBO calculations suggest the importance of the π-back-donation, as demonstrated by one of the leading donor-acceptor NBO interactions.

Table S2. Stabilization energies ($E^{(2)}$, in kJ mol^{-1}) of the leading donor-acceptor NBO interactions between the metal center and the thiadiene ligand for complexes **1**–**7**.

Complex	Fe→C^1-C^2	Fe-S→C^1-C^2 (Fe-S←C^1-C^2)	Fe-C^3→C^1-C^2 (Fe-C^3←C^1-C^2)
1	-105.9	-131.4 (-271.1)	-246.7 (-200.3)
2	-109.2	-131.0 (-278.2)	-252.0 (-207.5)
3	-108.6	-132.8 (-265.0)	-246.6 (-203.1)
4	-107.5	-132.8 (-268.2)	-232.5 (-211.2)
5	-108.2	-131.7 (-268.4)	-225.6 (-206.6)
6	-107.7	-131.3 (-265.8)	-237.9 (-213.6)
7	-108.5	-134.1 (-285.3)	-235.0 (-206.7)

In the NBO calculations we also included many other Lewis-like structures defined arbitrary by us (using the CHOOSE keyword) in order to check out different bonding patterns possible for **1**–**7**. Some of such structures were rejected by the NBO program due to the unfulfilled duodectet rule, others resulted in basis-set linear dependence issues. The structures that ended up successfully were analyzed by the natural resonance theory (NRT).[17] For these structures, the NRT analysis returned their zero percentage weights.

Section S4. Additional tables and figures

Table S3. Relative energies (ΔE, in kJ mol^{-1}) and interatomic distances (in pm) for complexes **1**–**6** in various electronic spin-states calculated at the ωB97X-D/def2-SVP level of theory.

Complex	State	ΔE	Fe-S	Fe-C^1	Fe-C^2	Fe-C^3
1	singlet	0.0	2.332	2.087	2.066	2.129
1	triplet	90.0	2.251	2.108	2.410	3.079
1	quintet	151.7	2.298	2.964	3.269	3.310
2	singlet	0.0	2.338	2.071	2.070	2.126
2	triplet	80.7	2.253	2.108	2.377	3.072
2	quintet	142.6	2.295	2.948	3.283	3.356
3	singlet	0.0	2.337	2.079	2.068	2.127
3	triplet	89.7	2.262	2.111	2.429	3.097
3	quintet	143.4	2.289	2.971	3.379	3.464
4	singlet	0.0	2.337	2.083	2.067	2.124
4	triplet	151.8	2.340	2.099	2.066	2.118
4	quintet	154.5	2.291	2.943	3.313	3.395
5	singlet	0.0	2.338	2.083	2.065	2.120
5	triplet	85.9	2.263	2.103	2.416	3.109
5	quintet	150.2	2.286	2.933	3.337	3.441
6	singlet	0.0	2.337	2.080	2.068	2.130
6	triplet	82.8	2.265	2.104	2.386	3.086
6	quintet	163.6	2.266	2.912	2.378	3.073

Table S4. QTAIM partial atomic charges (in *e*) of the atoms involved in the metal-ligand bonds in complexes **1**–**7**. The atomic charges on the S-C^1-C^2-C^3 atoms of free thiochalcone and 3-heptene-2-thione ligands are shown in parentheses.

Complex	Fe	S	C^1	C^2	C^3	C_{CO}
1	0.831	-0.185 (0.169)	-0.227 (-0.384)	-0.089 (-0.023)	-0.120 (-0.017)	1.024;1.040;1.040
2	0.831	-0.189 (0.158)	-0.230 (-0.379)	-0.084 (-0.019)	-0.097 (0.004)	1.019;1.038;1.049
3	0.833	-0.179 (0.142)	-0.207 (-0.340)	-0.087 (-0.023)	-0.117 (-0.015)	1.024;1.038;1.047
4	0.831	-0.196 (0.131)	-0.210 (-0.357)	-0.087 (-0.021)	-0.121 (-0.020)	1.022;1.037;1.043
5	0.831	-0.199 (0.121)	-0.208 (-0.354)	-0.080 (-0.012)	-0.099 (0.001)	1.030;1.035;1.043
6	0.830	-0.197 (0.125)	-0.208 (-0.354)	-0.085 (-0.017)	-0.099 (0.001)	1.023;1.035;1.044
7	0.823	-0.195 (0.189)	-0.232 (-0.407)	-0.092 (-0.031)	-0.121 (-0.024)	1.013;1.033;1.035

Table S5. QTAIM, SF and IQA parameters for the interaction between the Fe center and the thiochalcone ligand for complex **2**.

Parameter [a]	Fe-S	Fe-C^1	Fe-C^2	Fe-C^3	Fe-S-C^1	Fe-C^1-C^2	Fe-C^2-C^3
ρ [b]	0.070	0.087	0.084	0.079	0.070	0.083	0.079
$\nabla^2\rho$ [b]	0.168	0.217	0.249	0.202	0.180	0.264	0.235
H [b]	-0.020	-0.028	-0.025	-0.022	-0.019	-0.022	-0.020
$\lvert V\rvert/G$ [b]	1.32	1.34	1.29	1.31	1.29	1.25	1.25
SF(S-C^1-C^2-C^3) [b]	46.2	41.7	39.2	34.3	46.4	40.2	35.6
SF($Fe(CO)_3$) [b]	36.4	38.3	37.3	39.0	35.2	36.8	37.7
δ	0.638	0.469	0.389	0.514			
V_{cl}	-38.2	-150.9	-35.4	-79.0			
V_{xc}	-302.8	-267.0	-218.2	-278.9			
E_{inter}	-340.9	-417.9	-253.6	-357.9			

[a] ρ, $\nabla^2\rho$ and H are expressed in atomic units; SF is in percentage points; V_{cl}, V_{xc} and E_{inter} are given in kJ mol^{-1}. [b] Parameters calculated at the BCPs of Fe-S, Fe-C^1, Fe-C^2 and Fe-C^3 and at the RCPs of Fe-S-C^1, Fe-C^1-C^2 and Fe-C^2-C^3.

Table S6. QTAIM, SF and IQA parameters for the interaction between the Fe center and the thiochalcone ligand for complex **3**.

Parameter [a]	Fe-S	Fe-C^1	Fe-C^2	Fe-C^3	Fe-S-C^1	Fe-C^1-C^2	Fe-C^2-C^3
ρ [b]	0.070	0.085	0.084	0.080	0.070	0.083	0.080
$\nabla^2\rho$ [b]	0.164	0.218	0.244	0.202	0.183	0.261	0.239
H [b]	-0.020	-0.027	-0.026	-0.023	-0.018	-0.021	-0.020
$\lvert V\rvert/G$ [b]	1.33	1.33	1.30	1.31	1.28	1.24	1.25
SF(S-C^1-C^2-C^3) [b]	45.9	41.3	38.8	34.4	46.1	40.3	35.7
SF($Fe(CO)_3$) [b]	36.8	37.9	37.6	39.3	34.9	36.6	37.8
δ	0.638	0.452	0.392	0.522			
V_{cl}	-34.7	-141.3	-38.9	-85.1			
V_{xc}	-303.2	-256.3	-220.6	-283.4			
E_{inter}	-338.0	-397.6	-259.5	-368.4			

[a] ρ, $\nabla^2\rho$ and H are expressed in atomic units; SF is in percentage points; V_{cl}, V_{xc} and E_{inter} are given in kJ mol^{-1}. [b] Parameters calculated at the BCPs of Fe-S, Fe-C^1, Fe-C^2 and Fe-C^3 and at the RCPs of Fe-S-C^1, Fe-C^1-C^2 and Fe-C^2-C^3.

Table S7. QTAIM and IQA parameters for the interaction between the Fe center and the thiochalcone ligand for complex **4**.

Parameter [a]	Fe-S	Fe-C^1	Fe-C^2	Fe-C^3	Fe-S-C^1	Fe-C^1-C^2	Fe-C^2-C^3
ρ [b]	0.070	0.085	0.084	0.080	0.069	0.083	0.080
$\nabla^2\rho$ [b]	0.163	0.216	0.244	0.200	0.182	0.258	0.243
H [b]	-0.020	-0.027	-0.026	-0.023	-0.018	-0.022	-0.020
$\lvert V\rvert/G$ [b]	1.33	1.33	1.30	1.32	1.29	1.25	1.25
SF(S-C^1-C^2-C^3) [b]	45.7	41.3	38.7	34.3	46.0	40.3	35.7
SF($Fe(CO)_3$) [b]	36.8	37.8	37.6	39.3	34.8	36.7	37.7
δ	0.636	0.451	0.395	0.526			
V_{cl}	-42.9	-139.5	-39.0	-87.6			
V_{xc}	-302.9	-255.4	-222.3	-285.8			
E_{inter}	-345.8	-394.9	-261.3	-373.4			

[a] ρ, $\nabla^2\rho$ and H are expressed in atomic units; SF is in percentage points; V_{cl}, V_{xc} and E_{inter} are given in kJ mol^{-1}. [b] Parameters calculated at the BCPs of Fe-S, Fe-C^1, Fe-C^2 and Fe-C^3 and at the RCPs of Fe-S-C^1, Fe-C^1-C^2 and Fe-C^2-C^3.

Table S8. QTAIM and IQA parameters for the interaction between the Fe center and the thiochalcone ligand for complex **5**.

Parameter [a]	Fe-S	Fe-C^1	Fe-C^2	Fe-C^3	Fe-S-C^1	Fe-C^1-C^2	Fe-C^2-C^3
ρ [b]	0.070	0.085	0.084	0.081	0.069	0.083	0.080
$\nabla^2\rho$ [b]	0.163	0.217	0.243	0.201	0.181	0.258	0.247
H [b]	-0.020	-0.027	-0.026	-0.024	-0.018	-0.022	-0.020
$\lvert V\rvert/G$ [b]	1.33	1.33	1.30	1.32	1.28	1.25	1.25
SF(S-C^1-C^2-C^3) [b]	45.6	41.3	38.7	34.1	45.9	40.3	35.6
SF($Fe(CO)_3$) [b]	36.7	37.7	37.6	39.5	34.7	36.7	37.6
δ	0.638	0.448	0.394	0.523			
V_{cl}	-44.6	-138.1	-32.2	-82.1			
V_{xc}	-303.3	-254.1	-221.7	-287.1			
E_{inter}	-347.9	-392.1	-253.9	-369.2			

[a] ρ, $\nabla^2\rho$ and H are expressed in atomic units; SF is in percentage points; V_{cl}, V_{xc} and E_{inter} are given in kJ mol^{-1}. [b] Parameters calculated at the BCPs of Fe-S, Fe-C^1, Fe-C^2 and Fe-C^3 and at the RCPs of Fe-S-C^1, Fe-C^1-C^2 and Fe-C^2-C^3.

Table S9. QTAIM and IQA parameters for the interaction between the Fe center and the thiochalcone ligand for complex **6**.

Parameter [a]	Fe-S	Fe-C^1	Fe-C^2	Fe-C^3	Fe-S-C^1	Fe-C^1-C^2	Fe-C^2-C^3
ρ [b]	0.070	0.085	0.084	0.079	0.070	0.083	0.079
$\nabla^2\rho$ [b]	0.164	0.215	0.244	0.202	0.181	0.259	0.239
H [b]	-0.020	-0.027	-0.026	-0.023	-0.018	-0.022	-0.020
$\lvert V\rvert/G$ [b]	1.33	1.33	1.30	1.31	1.29	1.25	1.25
SF($_{S\text{-}C^1\text{-}C^2\text{-}C^3}$) [b]	45.7	41.3	38.7	34.1	45.9	40.2	35.4
SF($_{Fe(CO)_3}$) [b]	36.7	37.9	37.6	39.2	34.9	36.7	37.7
δ	0.636	0.453	0.393	0.516			
V_{cl}	-43.3	-138.5	-36.8	-79.9			
V_{xc}	-302.9	-257.1	-221.0	-281.2			
E_{inter}	-346.2	-395.5	-257.7	-361.0			

[a] ρ, $\nabla^2\rho$ and H are expressed in atomic units; SF is in percentage points; V_{cl}, V_{xc} and E_{inter} are given in kJ mol^{-1}. [b] Parameters calculated at the BCPs of Fe-S, Fe-C^1, Fe-C^2 and Fe-C^3 and at the RCPs of Fe-S-C^1, Fe-C^1-C^2 and Fe-C^2-C^3.

Table S10. QTAIM and SF parameters for the interaction between the Fe center and the thiadiene ligand for complexes **1** and **7** (in parentheses).

Parameter [a,b]	Fe-S-C^1	Fe-C^1-C^2	Fe-C^2-C^3
ρ	0.070 (0.069)	0.082 (0.084)	0.079 (0.081)
$\nabla^2\rho$	0.186 (0.177)	0.258 (0.264)	0.233 (0.251)
H	-0.018 (-0.019)	-0.021 (-0.022)	-0.021 (-0.021)
SF($_{S\text{-}C^1\text{-}C^2\text{-}C^3}$)	46.4 (47.2)	40.7 (41.3)	35.5 (37.4)
SF($_{Fe(CO)_3}$)	34.5 (35.3)	36.5 (36.8)	38.0 (37.7)

[a] ρ, $\nabla^2\rho$ and H are expressed in atomic units; SF is in percentage points. [b] Parameters calculated at the RCPs of Fe-S-C^1, Fe-C^1-C^2 and Fe-C^2-C^3.

Table S11. QTAIM, SF and IQA parameters of bonds for the S-C^1-C^2-C^3 fragment of complex **2**. The corresponding bond lengths in the free thiochalcone ligand are shown in parentheses.

Parameter [a]	S-C^1	C^1-C^2	C^2-C^3
ρ	0.200 (0.235)	0.302 (0.280)	0.301 (0.345)
$\nabla^2\rho$	-0.361 (-0.267)	-0.824 (-0.765)	-0.831 (-1.063)
H	-0.170 (-0.286)	-0.308 (-0.267)	-0.307 (-0.395)
$\lvert V\rvert/G$	3.13 (2.30)	4.01 (4.52)	4.09 (4.05)
SF(S-C^1-C^2-C^3)	88.4 (94.2)	88.2 (90.4)	86.3 (90.2)
SF($Fe(CO)_3$)	4.1	3.1	2.9
δ	1.253 (1.744)	1.247 (1.683)	1.219 (1.596)
V_{cl}	-18.6 (-520.4)	93.3 (70.2)	90.4 (144.0)
V_{xc}	-856.6 (-1117.2)	-1008.9 (-911.2)	-991.6 (-1225.6)
E_{inter}	-875.2 (-1637.6)	-915.6 (-840.9)	-901.1 (-1081.6)

[a] ρ, $\nabla^2\rho$ and H are expressed in atomic units; SF in percentage points; V_{cl}, V_{xc} and E_{inter} are given in kJ mol^{-1}.

Table S12. QTAIM, SF and IQA parameters of bonds for the S-C^1-C^2-C^3 fragment of complex **3**. The corresponding bond lengths in the free thiochalcone ligand are shown in parentheses.

Parameter [a]	S-C^1	C^1-C^2	C^2-C^3
ρ	0.200 (0.233)	0.302 (0.278)	0.301 (0.347)
$\nabla^2\rho$	-0.362 (-0.253)	-0.826 (-0.759)	-0.830 (-1.073)
H	-0.172 (-0.282)	-0.308 (-0.264)	-0.308 (-0.400)
$\lvert V\rvert/G$	3.11 (2.29)	4.03 (4.56)	4.07 (4.03)
SF(S-C^1-C^2-C^3)	88.3 (94.1)	88.1 (90.2)	86.3 (90.4)
SF($Fe(CO)_3$)	4.0	3.1	3.0
δ	1.249 (1.712)	1.242 (1.127)	1.224 (1.629)
V_{cl}	-25.3 (-497.6)	92.6 (69.9)	90.1 (146.7)
V_{xc}	-854.4 (-1100.6)	-1006.4 (-900.3)	-993.7 (-1244.5)
E_{inter}	-879.7 (-1598.2)	-913.8 (-830.5)	-903.6 1097.8)

[a] ρ, $\nabla^2\rho$ and H are expressed in atomic units; SF in percentage points; V_{cl}, V_{xc} and E_{inter} are given in kJ mol^{-1}.

Table S13. QTAIM, SF and IQA parameters of bonds for the S-C^1-C^2-C^3 fragment of complex **4**. The corresponding bond lengths in the free thiochalcone ligand are shown in parentheses.

Parameter [a]	S-C^1	C^1-C^2	C^2-C^3
ρ	0.201 (0.234)	0.303 (0.278)	0.300 (0.348)
$\nabla^2\rho$	-0.366 (-0.258)	-0.833 (-0.761)	-0.828 (-1.074)
H	-0.172 (-0.284)	-0.311 (-0.264)	-0.307 (-0.401)
$\lvert V\rvert/G$	3.14 (2.29)	4.04 (4.57)	4.07 (4.03)
SF(S-C^1-C^2-C^3)	88.2 (94.0)	88.1 (90.1)	86.2 (90.3)
SF($Fe(CO)_3$)	4.0	3.1	3.0
δ	1.248 (1.725)	1.246 (1.123)	1.220 (1.632)
V_{cl}	-17.3 (-504.9)	94.0 (70.0)	90.1 (146.7)
V_{xc}	-855.3 (-1108.5)	-1010.2 (-898.5)	-991.3 (-1247.0)
E_{inter}	-872.6 (-1613.4)	-916.2 (-828.5)	901.2 (1100.3)

[a] ρ, $\nabla^2\rho$ and H are expressed in atomic units; SF in percentage points; V_{cl}, V_{xc} and E_{inter} are given in kJ mol^{-1}.

Table S14. QTAIM, SF and IQA parameters of bonds for the S-C^1-C^2-C^3 fragment of complex **5**. The corresponding bond lengths in the free thiochalcone ligand are shown in parentheses.

Parameter [a]	S-C^1	C^1-C^2	C^2-C^3
ρ	0.200 (0.234)	0.304 (0.280)	0.298 (0.345)
$\nabla^2\rho$	-0.365 (-0.263)	-0.839 (-0.769)	-0.817 (-1.064)
H	-0.171 (-0.283)	-0.313 (-0.267)	-0.303 (-0.397)
$\lvert V\rvert/G$	3.14 (2.30)	4.04 (4.56)	4.07 (4.03)
SF(S-C^1-C^2-C^3)	88.2 (94.0)	88.1 (90.2)	86.0 (90.0)
SF($Fe(CO)_3$)	4.0	3.0	3.0
δ	1.245 (1.716)	1.250 (1.132)	1.207 (1.601)
V_{cl}	-16.7 (-496.0)	94.0 (69.6)	88.8 (145.2)
V_{xc}	-853.7 (-1104.2)	-1014.2 (-905.9)	-981.4 (-1229.0)
E_{inter}	-870.3 (-1600.2)	-920.1 (-836.2)	-892.6 (-1083.9)

[a] ρ, $\nabla^2\rho$ and H are expressed in atomic units; SF in percentage points; V_{cl}, V_{xc} and E_{inter} are given in kJ mol^{-1}.

Table S15. QTAIM, SF and IQA parameters of bonds for the S-C^1-C^2-C^3 fragment of complex **6**. The corresponding bond lengths in the free thiochalcone ligand are shown in parentheses.

Parameter [a]	S-C^1	C^1-C^2	C^2-C^3
ρ	0.200 (0.234)	0.303 (0.280)	0.300 (0.346)
$\nabla^2\rho$	-0.364 (-0.260)	-0.835 (-0.768)	-0.827 (-1.067)
H	-0.171 (-0.284)	-0.311 (-0.267)	-0.306 (-0.398)
$\lvert V\rvert/G$	3.14 (2.30)	4.04 (4.55)	4.08 (4.04)
SF(S-C^1-C^2-C^3)	88.2 (94.0)	88.1 (90.1)	86.2 (90.1)
SF($Fe(CO)_3$)	4.0	3.1	3.0
δ	1.245 (1.718)	1.245 (1.131)	1.217 (1.606)
V_{cl}	-17.2 (-500.1)	94.0 (70.8)	90.2 (145.5)
V_{xc}	-853.7 (-1105.2)	-1010.5 (-905.6)	-989.8 (-1233.2)
E_{inter}	-870.9 (-1605.3)	-916.5 (-834.8)	-899.7 (-1087.7)

[a] ρ, $\nabla^2\rho$ and H are expressed in atomic units; SF in percentage points; V_{cl}, V_{xc} and E_{inter} are given in kJ mol^{-1}.

Table S16. QTAIM, SF and IQA parameters of bonds for the S-C^1-C^2-C^3 fragment of complex **7**. The corresponding bond lengths in the free thiadiene ligand are shown in parentheses.

Parameter [a]	S-C^1	C^1-C^2	C^2-C^3
ρ	0.202 (0.239)	0.303 (0.278)	0.301 (0.350)
$\nabla^2\rho$	-0.369 (-0.233)	-0.833 (-0.760)	-0.831 (-1.083)
H	-0.172 (-0.294)	-0.311 (-0.263)	-0.308 (-0.407)
$\lvert V\rvert/G$	3.15 (2.25)	4.03 (4.60)	4.06 (3.99)
SF(S-C^1-C^2-C^3)	88.8 (94.7)	88.5 (90.7)	86.5 (90.7)
SF($Fe(CO)_3$)	4.0	3.1	3.1
δ	1.268 (1.829)	1.259 (1.122)	1.229 (1.688)
V_{cl}	-14.9 (-583.1)	94.9 (68.8)	88.7 (148.6)
V_{xc}	-865.8 (-1158.1)	-1016.4 (-895.4)	-995.8 (-1276.0)
E_{inter}	-880.6 (-1741.2)	-921.5 (-826.6)	-907.2 (-1127.4)

[a] ρ, $\nabla^2\rho$ and H are expressed in atomic units; SF in percentage points; V_{cl}, V_{xc} and E_{inter} are given in kJ mol^{-1}.

Table S17. Leading atomic contributions (in percentage points) to three frontier molecular orbitals of free thiadiene ligands. [a]

Ligand	HOMO-1	HOMO	LUMO
$Ar^1 = Ar^2$ = phenyl	S (38.1) C^2 (17.0)	S (80.8) C^2 (4.6)	S (27.0) C^1 (21.6) C^3 (18.4) C^2 (4.0)
Ar^1 = phenyl; Ar^2 = 2-thienyl	S (45.4) C^2 (14.4)	S (69.0) C^2 (7.9)	S (25.8) C^1 (20.3) C^3 (18.1) C^2 (4.3)
Ar^1 = 2-thienyl; Ar^2 = phenyl	S (39.6) C^2 (13.0)	S (92.2) C^2 (2.6)	S (25.9) C^1 (20.4) C^3 (16.5) C^2 (3.0)
Ar^1 = ferrocenyl; Ar^2 = phenyl	Fe (55.9) S (26.1)	S (78.6) Fe (11.2)	S (24.8) C^1 (21.1) C^3 (19.0) C^2 (5.1)
Ar^1 = ferrocenyl; Ar^2 = 2-furyl	S (43.7) C^2 (14.5)	S (65.7) Fe (11.8)	S (25.2) C^1 (21.6) C^3 (19.1) C^2 (5.1)
Ar^1 = ferrocenyl; Ar^2 = 2-thienyl	S (40.3) C^2 (15.3)	S (72.9) Fe (12.6)	S (23.6) C^1 (19.7) C^3 (18.4) C^2 (5.6)
$Ar^1 = Ar^2$ = methyl	S (42.5) C^3 (21.9) C^2 (21.1)	S (91.5) C^2 (2.6)	S (31.6) C^1 (32.3) C^3 (25.0) C^2 (3.2)

[a] Molecular orbital composition was analyzed in terms of natural atomic orbitals for the ωB97X-D/def2-SVP wave functions of free thiadiene ligands in their ωB97X-D/def2-SVP-optimized geometries.

Table S18. Energies (in eV) of three frontier molecular orbitals for free thiadiene ligands. [a]

Ligand	HOMO-1	HOMO	LUMO
$Ar^1 = Ar^2$ = phenyl	-8.27	-7.91	-1.16
Ar^1 = phenyl; Ar^2 = 2-thienyl	-8.10	-7.89	-1.22
Ar^1 = 2-thienyl; Ar^2 = phenyl	-8.12	-8.02	-1.27
Ar^1 = ferrocenyl; Ar^2 = phenyl	-8.03	-7.80	-0.97
Ar^1 = ferrocenyl; Ar^2 = 2-furyl	-7.87	-7.75	-0.94
Ar^1 = ferrocenyl; Ar^2 = 2-thienyl	-7.95	-7.79	-1.03
$Ar^1 = Ar^2$ = methyl	-8.74	-7.88	-0.44

[a] The energies were calculated at the ωB97X-D/def2-SVP level of theory.

Table S19. Selected atomic contributions (in percentage points) to two pairs of NOCVs involved in two leading orbital interactions for complexes **1**–**7**. The pairwise NOCV interactions are also characterized by their interaction energy (ΔE_{orb}, in kJ mol^{-1}).

Complex	ΔE_{orb}	NOCV	NOCV	ΔE_{orb}	NOCV	NOCV
1	-764.1	S (23.5) C^1 (18.6) C^2 (6.0) C^3 (28.7) Fe (7.4)	S (2.2) C^1 (8.7) C^2 (0.7) C^3 (11.2) Fe (55.5)	-356.0	S (42.4) C^1 (4.1) C^2 (13.4) C^3 (4.8) Fe (23.2)	S (3.3) C^1 (3.1) C^2 (1.6) C^3 (4.1) Fe (70.6)
2	-780.4	S (21.0) C^1 (22.0) C^2 (5.6) C^3 (26.6) Fe (7.6)	S (1.6) C^1 (9.6) C^2 (0.6) C^3 (11.2) Fe (55.0)	-344.1	S (40.8) C^1 (1.9) C^2 (13.6) C^3 (4.3) Fe (23.6)	S (3.0) C^1 (4.1) C^2 (2.7) C^3 (4.7) Fe (69.5)
3	-776.8	S (21.5) C^1 (19.3) C^2 (6.5) C^3 (28.6) Fe (7.8)	S (1.7) C^1 (9.2) C^2 (0.7) C^3 (11.5) Fe (55.1)	-346.3	S (43.0) C^1 (2.5) C^2 (14.2) C^3 (4.4) Fe (24.3)	S (3.1) C^1 (3.5) C^2 (2.1) C^3 (4.6) Fe (69.4)
4	-768.5	S (20.6) C^1 (18.6) C^2 (6.4) C^3 (27.4) Fe (6.8)	S (1.8) C^1 (9.2) C^2 (0.8) C^3 (11.6) Fe (54.5)	-349.7	S (41.8) C^1 (3.1) C^2 (13.1) C^3 (4.3) Fe (23.2)	S (3.4) C^1 (3.9) C^2 (1.8) C^3 (4.0) Fe (67.8)
5	-763.2	S (21.1) C^1 (17.9) C^2 (5.8) C^3 (26.9) Fe (6.0)	S (2.2) C^1 (8.8) C^2 (0.8) C^3 (10.9) Fe (55.0)	-355.1	S (41.0) C^1 (4.3) C^2 (13.7) C^3 (5.0) Fe (22.8)	S (3.4) C^1 (4.0) C^2 (1.4) C^3 (3.4) Fe (69.5)
6	-764.8	S (20.3) C^1 (18.7) C^2 (5.9) C^3 (26.6) Fe (6.8)	S (1.8) C^1 (9.2) C^2 (0.7) C^3 (11.3) Fe (54.8)	-347.6	S (42.1) C^1 (3.3) C^2 (13.3) C^3 (4.2) Fe (23.4)	S (3.3) C^1 (4.1) C^2 (2.1) C^3 (4.0) Fe (68.4)
7	-753.0	S (24.6) C^1 (22.0) C^2 (6.1) C^3 (29.6) Fe (8.0)	S (2.0) C^1 (9.5) C^2 (0.5) C^3 (12.5) Fe (54.4)	-359.5	S (42.6) C^1 (3.6) C^2 (14.6) C^3 (5.5) Fe (25.2)	S (3.1) C^1 (2.4) C^2 (1.5) C^3 (4.4) Fe (74.4)

Table S20. WBI for selected pairs of atoms in complexes **1**–**7** and the corresponding free thiadiene ligands (in parentheses).

Complex	Fe-S	Fe-C^1	Fe-C^2	Fe-C^3	S-C^1	C^1-C^2	C^2-C^3
1	0.442	0.270	0.193	0.370	1.166 (1.741)	1.324 (1.110)	1.275 (1.735)
2	0.442	0.264	0.191	0.369	1.169 (1.730)	1.331 (1.118)	1.263 (1.708)
3	0.434	0.266	0.192	0.372	1.154 (1.683)	1.313 (1.103)	1.277 (1.737)
4	0.433	0.265	0.193	0.374	1.160 (1.703)	1.320 (1.101)	1.272 (1.743)
5	0.433	0.262	0.195	0.371	1.158 (1.694)	1.323 (1.108)	1.261 (1.714)
6	0.432	0.266	0.192	0.367	1.158 (1.696)	1.318 (1.108)	1.272 (1.719)
7	0.436	0.282	0.195	0.397	1.176 (1.802)	1.334 (1.100)	1.287 (1.801)

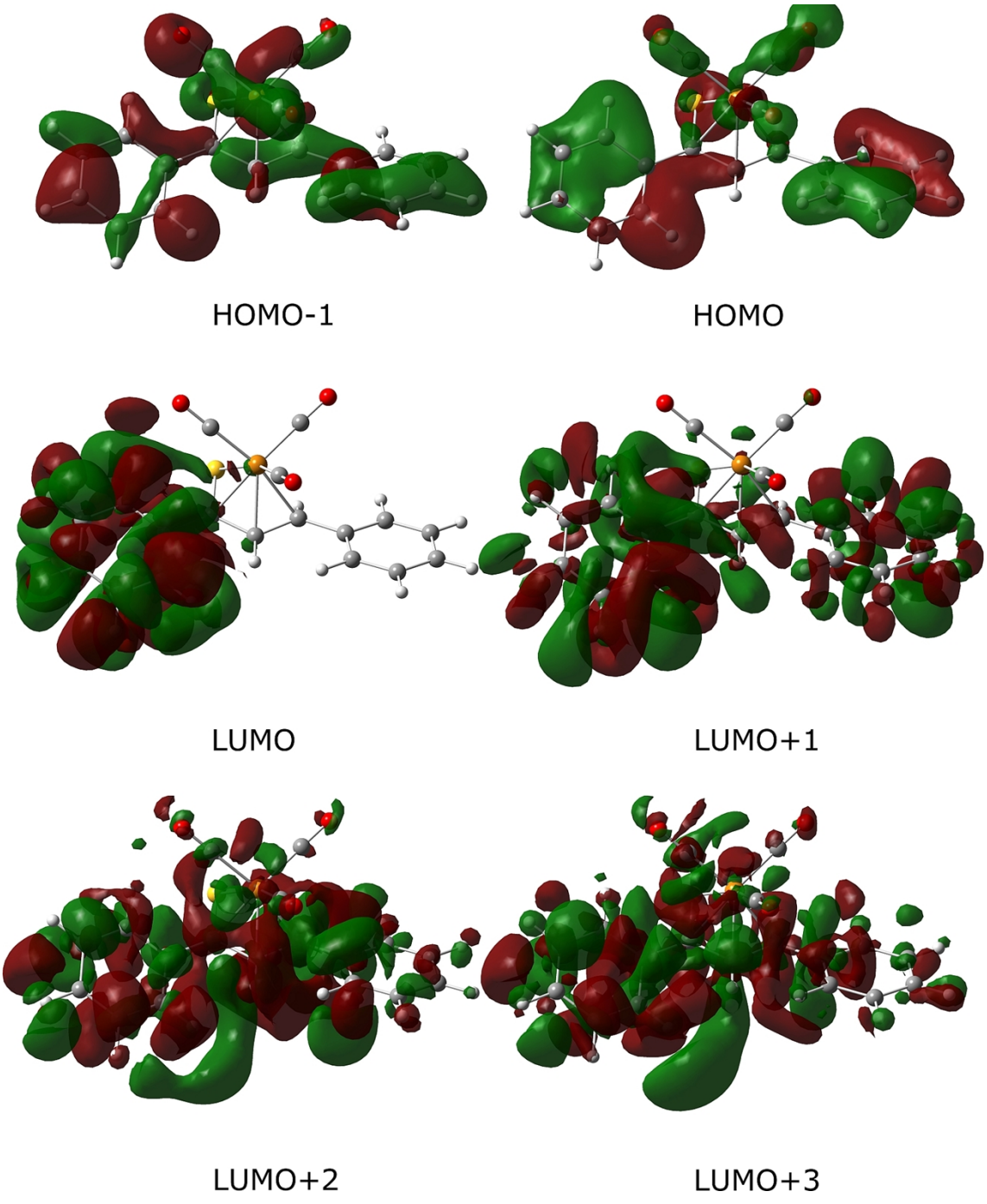

Figure S4. Orbitals included in the active space of CASSCF calculation for complex **1**. The contours are plotted with an isovalue of 0.02 a.u. Color codes for elements are explained in Figure 2.

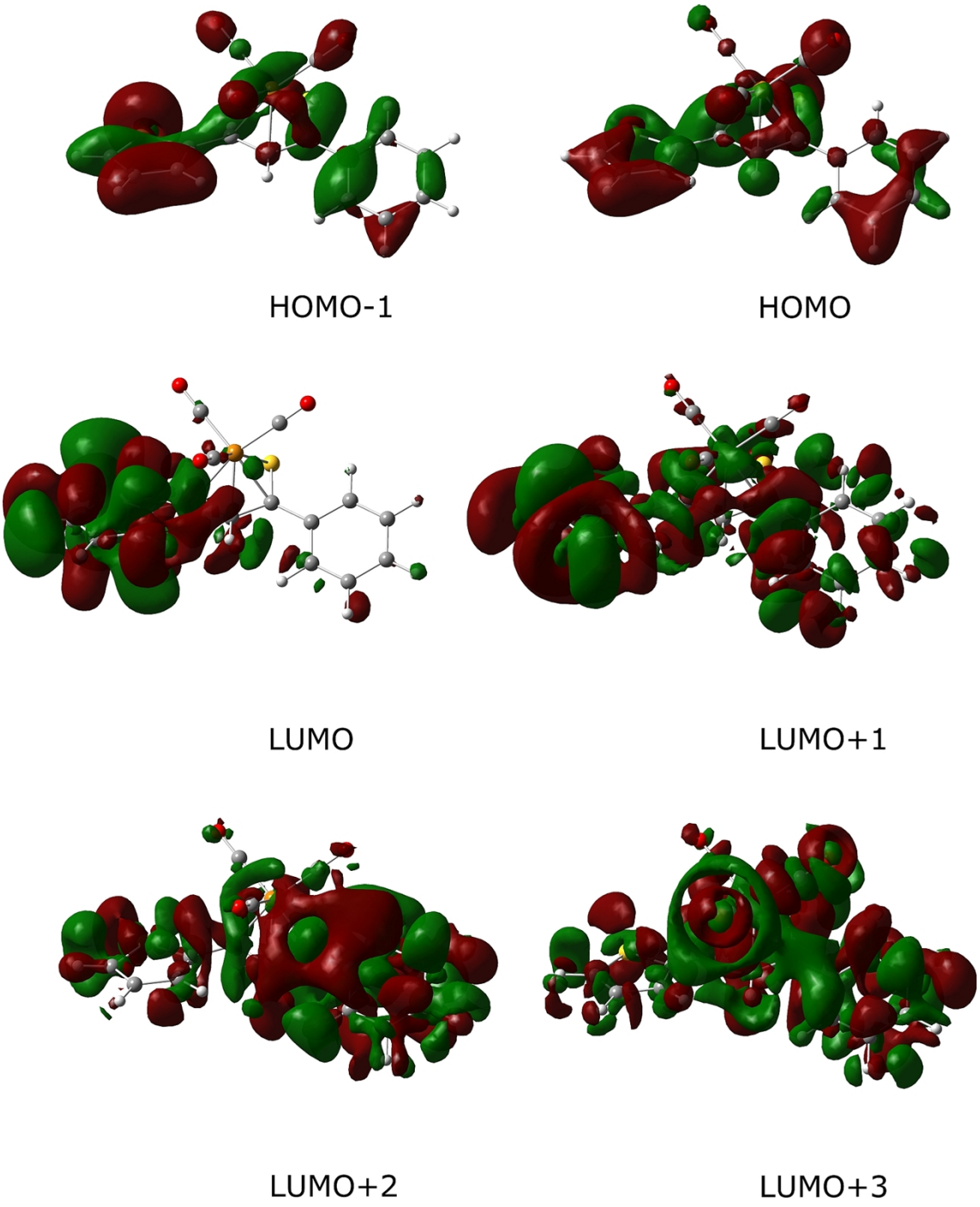

Figure S5. Orbitals included in the active space of CASSCF calculation for complex **2**. The contours are plotted with an isovalue of 0.02 a.u. Color codes for elements are explained in Figure 2.

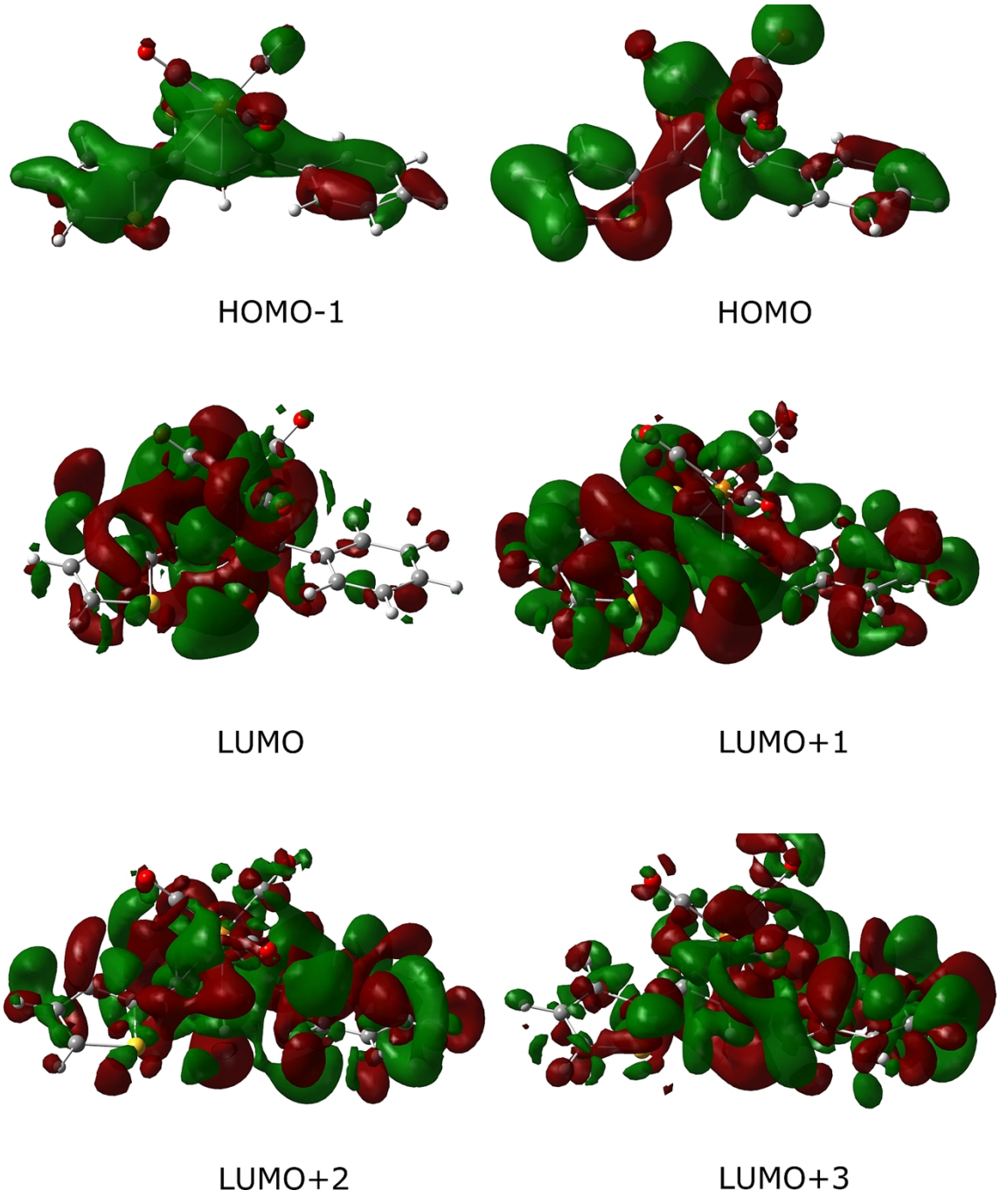

Figure S6. Orbitals included in the active space of CASSCF calculation for complex **3**. The contours are plotted with an isovalue of 0.02 a.u. Color codes for elements are explained in Figure 2.

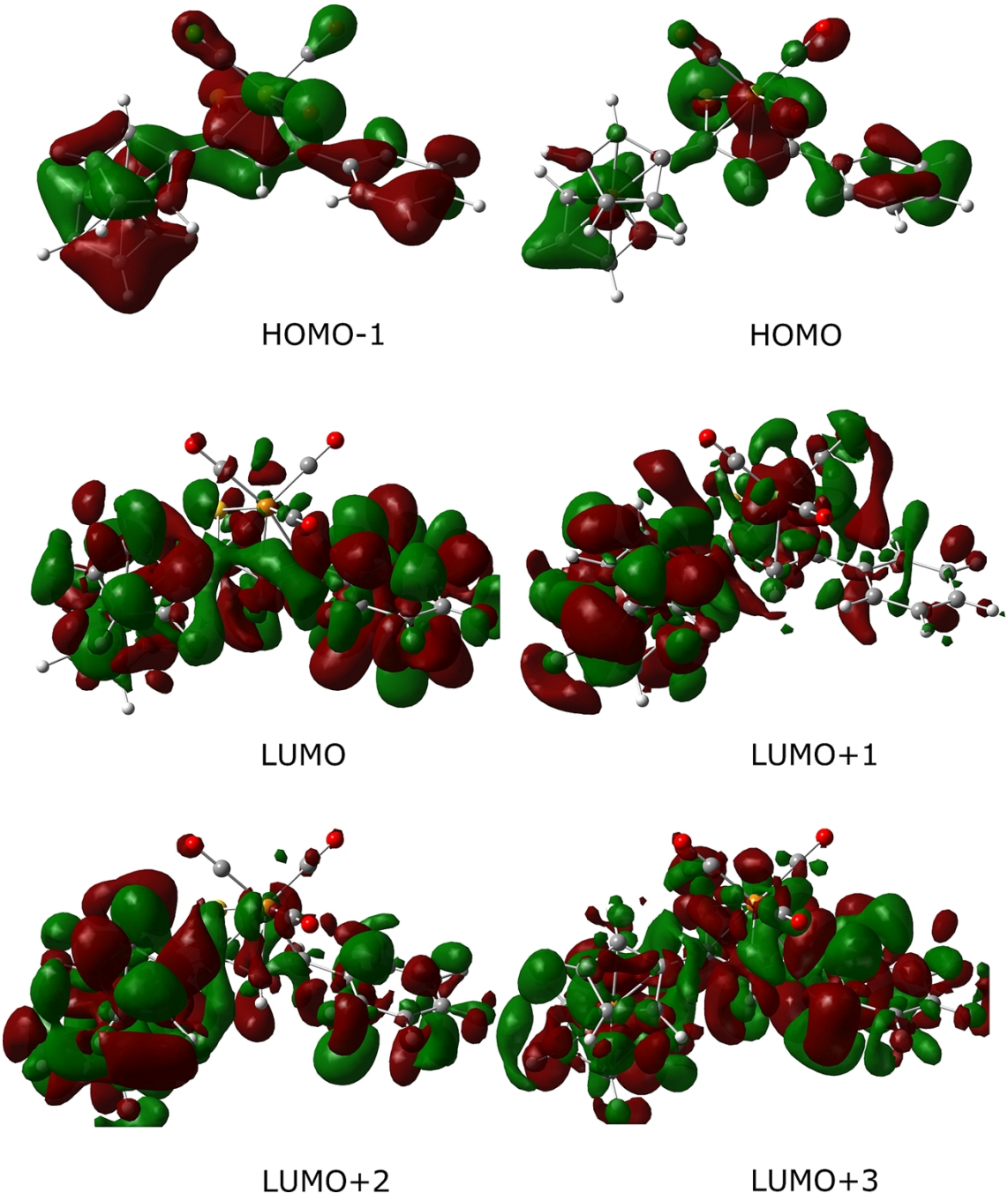

Figure S7. Orbitals included in the active space of CASSCF calculation for complex **4**. The contours are plotted with an isovalue of 0.02 a.u. Color codes for elements are explained in Figure 2.

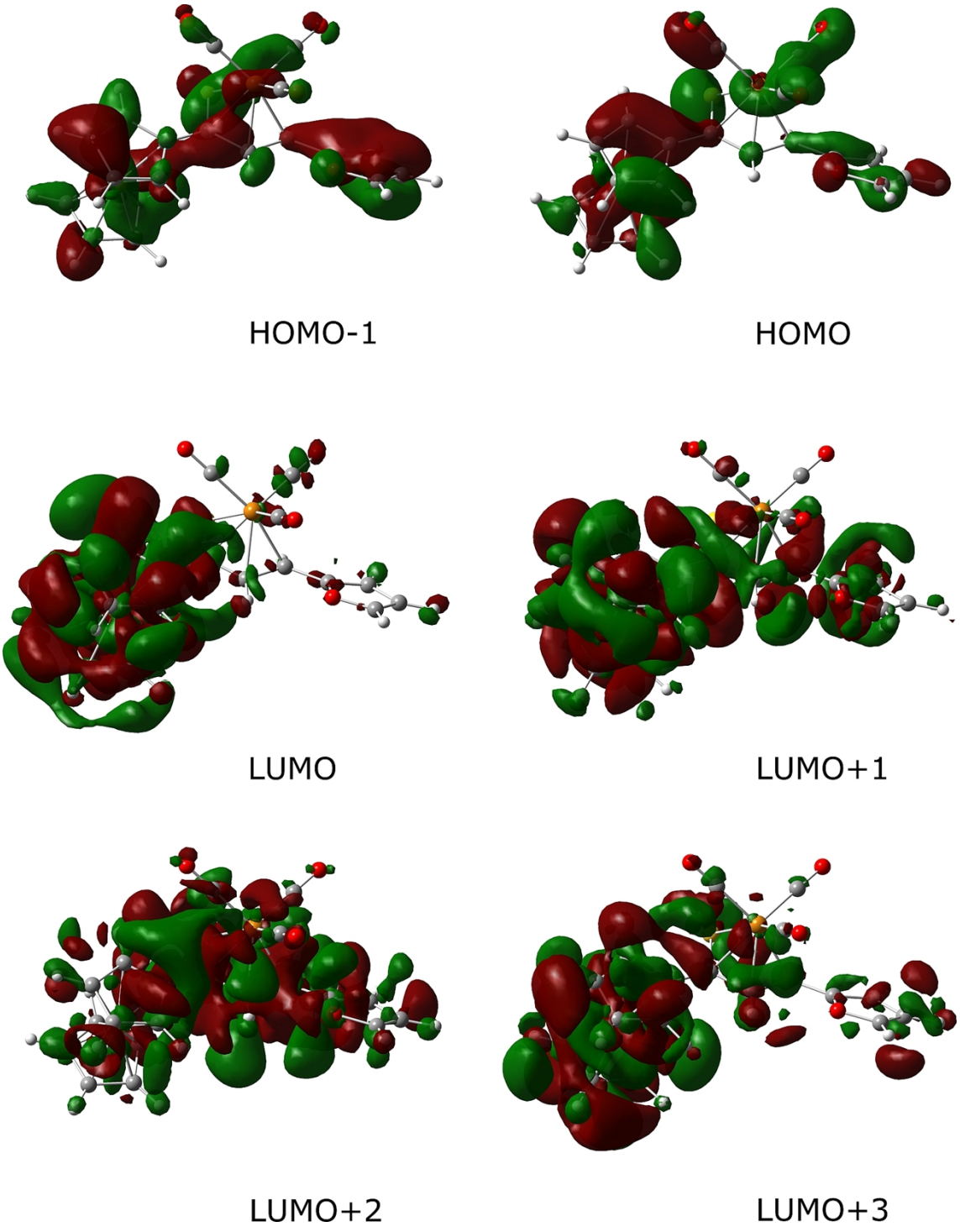

Figure S8. Orbitals included in the active space of CASSCF calculation for complex **5**. The contours are plotted with an isovalue of 0.02 a.u. Color codes for elements are explained in Figure 2.

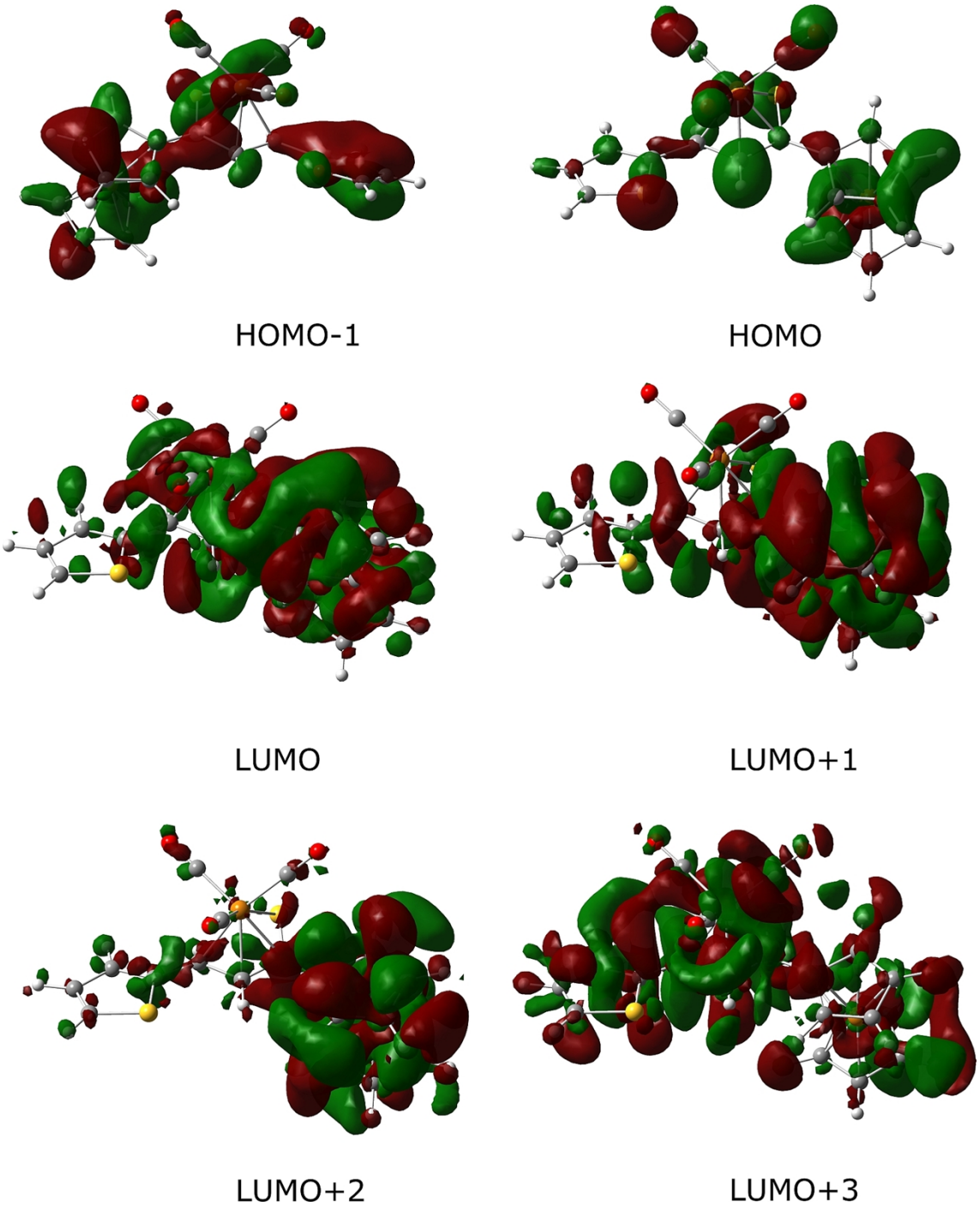

Figure S9. Orbitals included in the active space of CASSCF calculation for complex **6**. The contours are plotted with an isovalue of 0.02 a.u. Color codes for elements are explained in Figure 2.

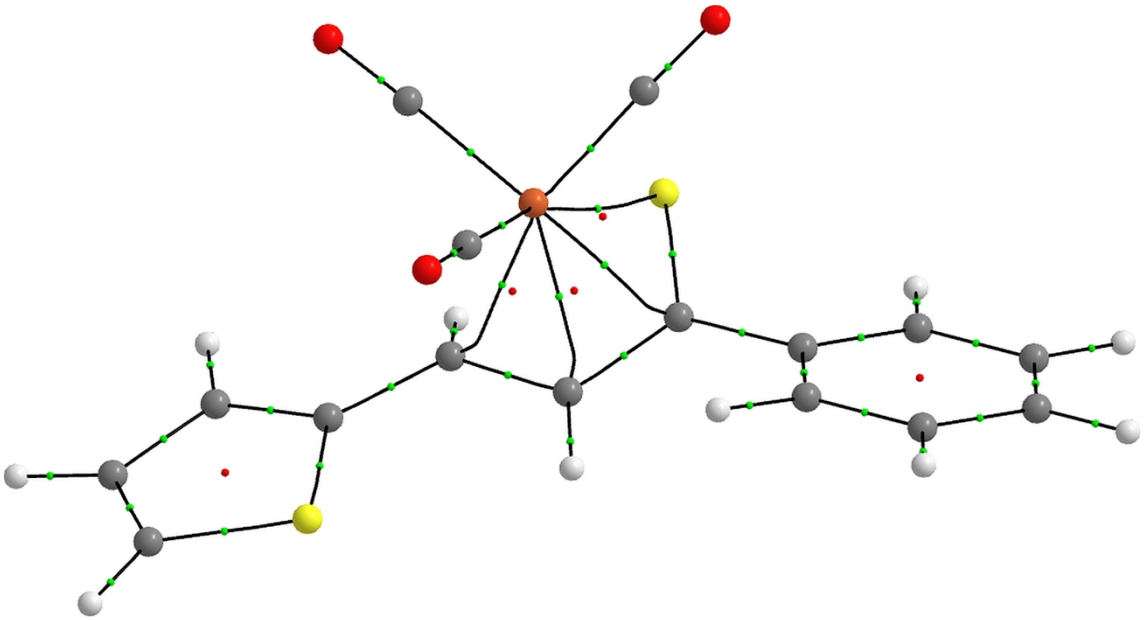

Figure S10. QTAIM molecular graph of complex **2**. Bond paths are drawn with black lines. Bond critical points are shown as small green spheres, and ring critical points as small red spheres. Color codes for elements are explained in Figure 2.

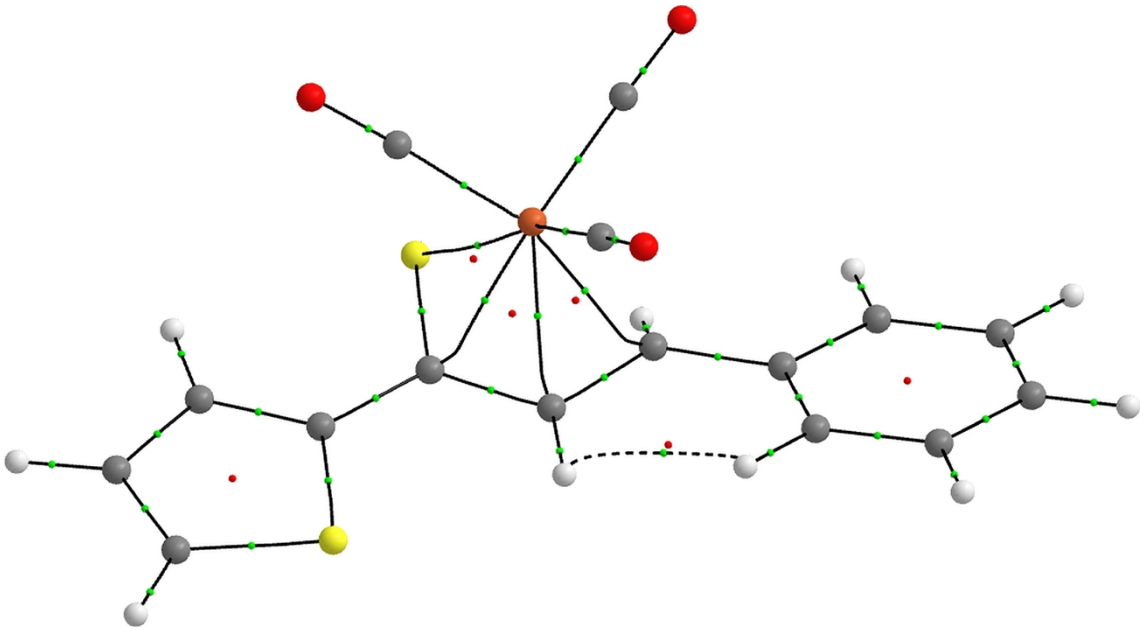

Figure S11. QTAIM molecular graph of complex **3**. Bond paths are drawn with black lines. Bond critical points are shown as small green spheres, and ring critical points as small red spheres. Color codes for elements are explained in Figure 2.

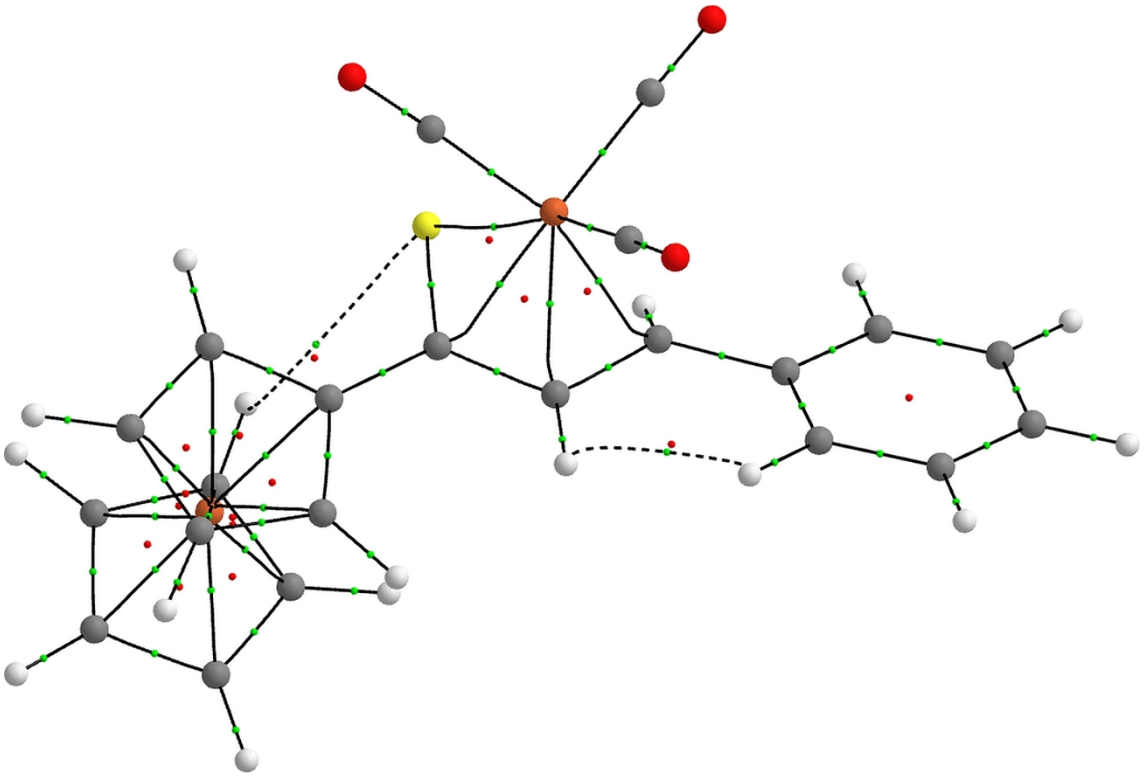

Figure S12. QTAIM molecular graph of complex **4**. Bond paths are drawn with black lines. Bond critical points are shown as small green spheres, and ring critical points as small red spheres. Color codes for elements are explained in Figure 2.

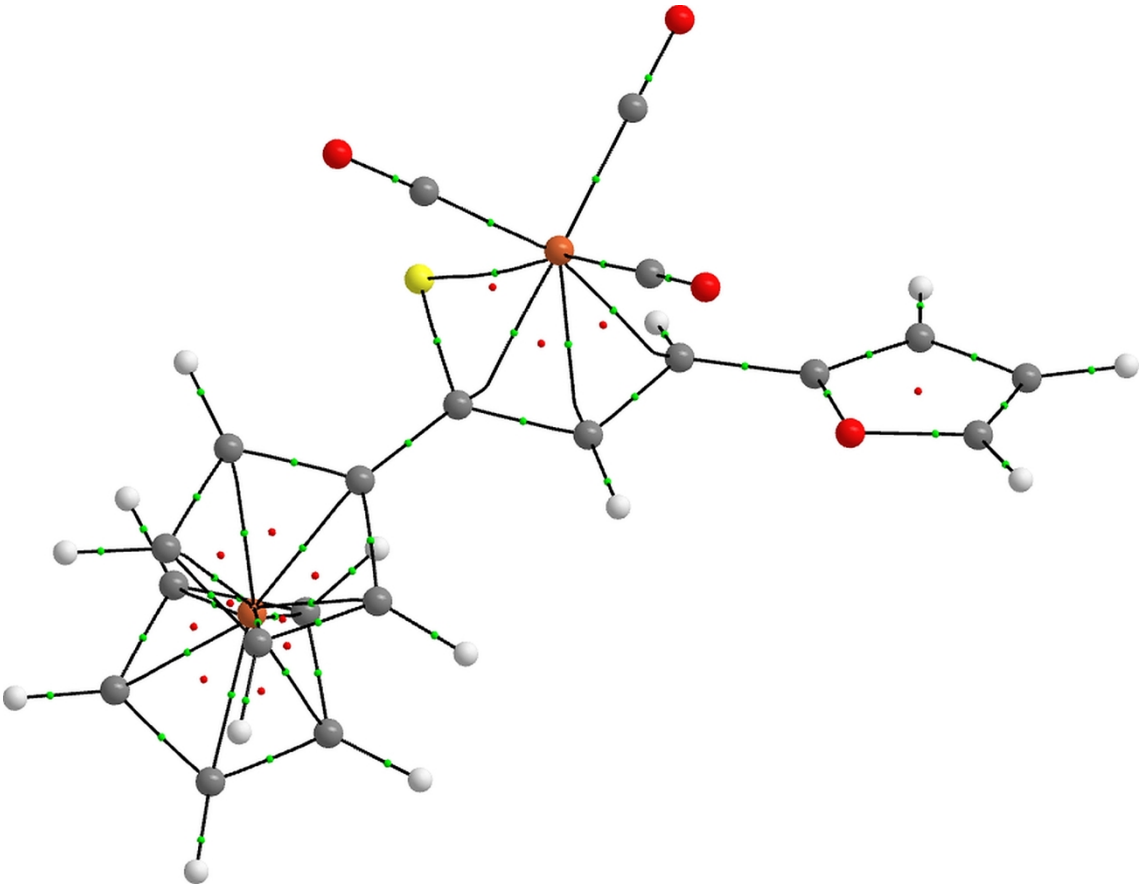

Figure S13. QTAIM molecular graph of complex **5**. Bond paths are drawn with black lines. Bond critical points are shown as small green spheres, and ring critical points as small red spheres. Color codes for elements are explained in Figure 2.

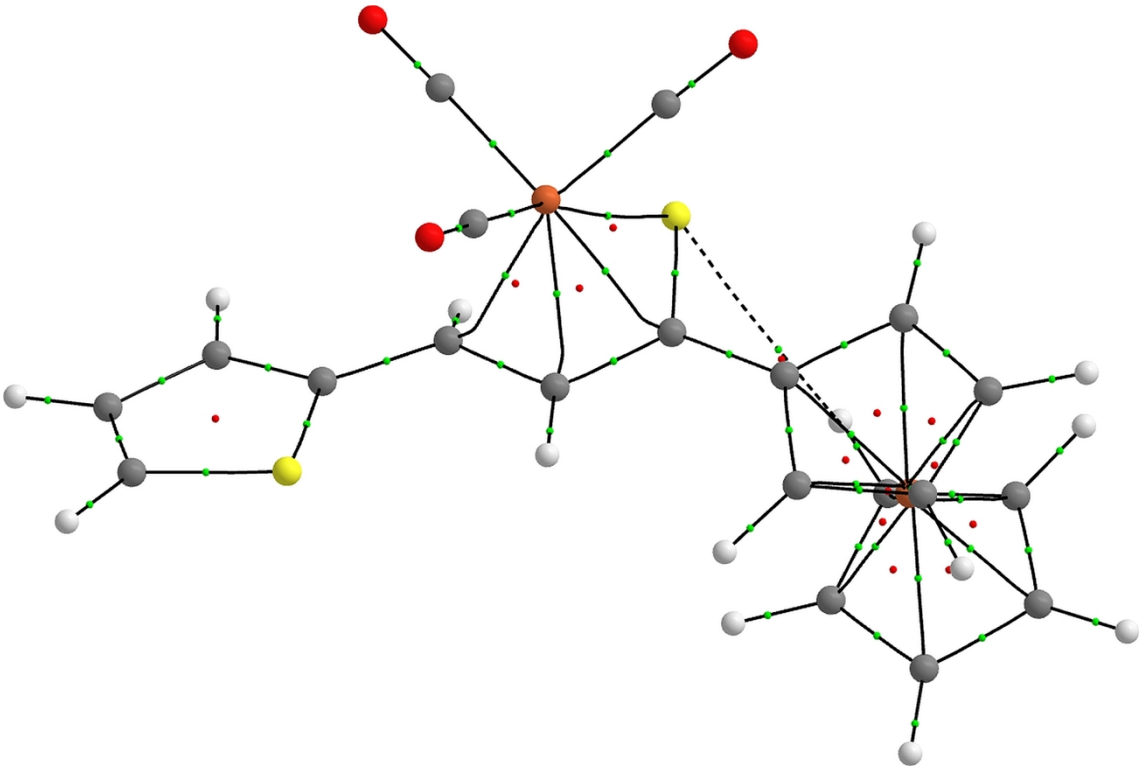

Figure S14. QTAIM molecular graph of complex **6**. Bond paths are drawn with black lines. Bond critical points are shown as small green spheres, and ring critical points as small red spheres. Color codes for elements are explained in Figure 2.

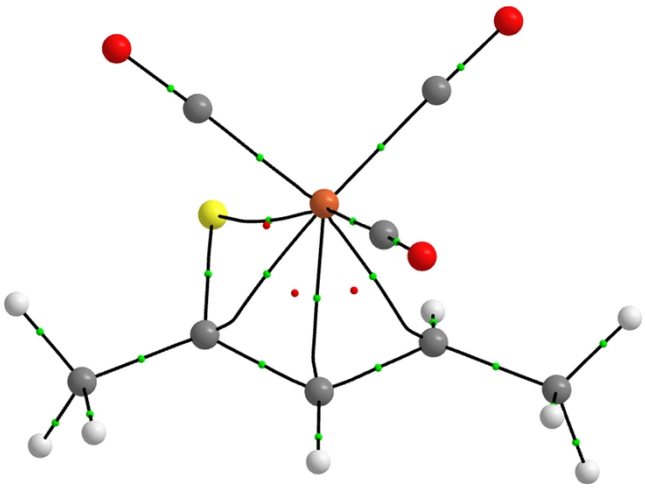

Figure S15. QTAIM molecular graph of complex **7**. Bond paths are drawn with black lines. Bond critical points are shown as small green spheres, and ring critical points as small red spheres. Color codes for elements are explained in Figure 2.

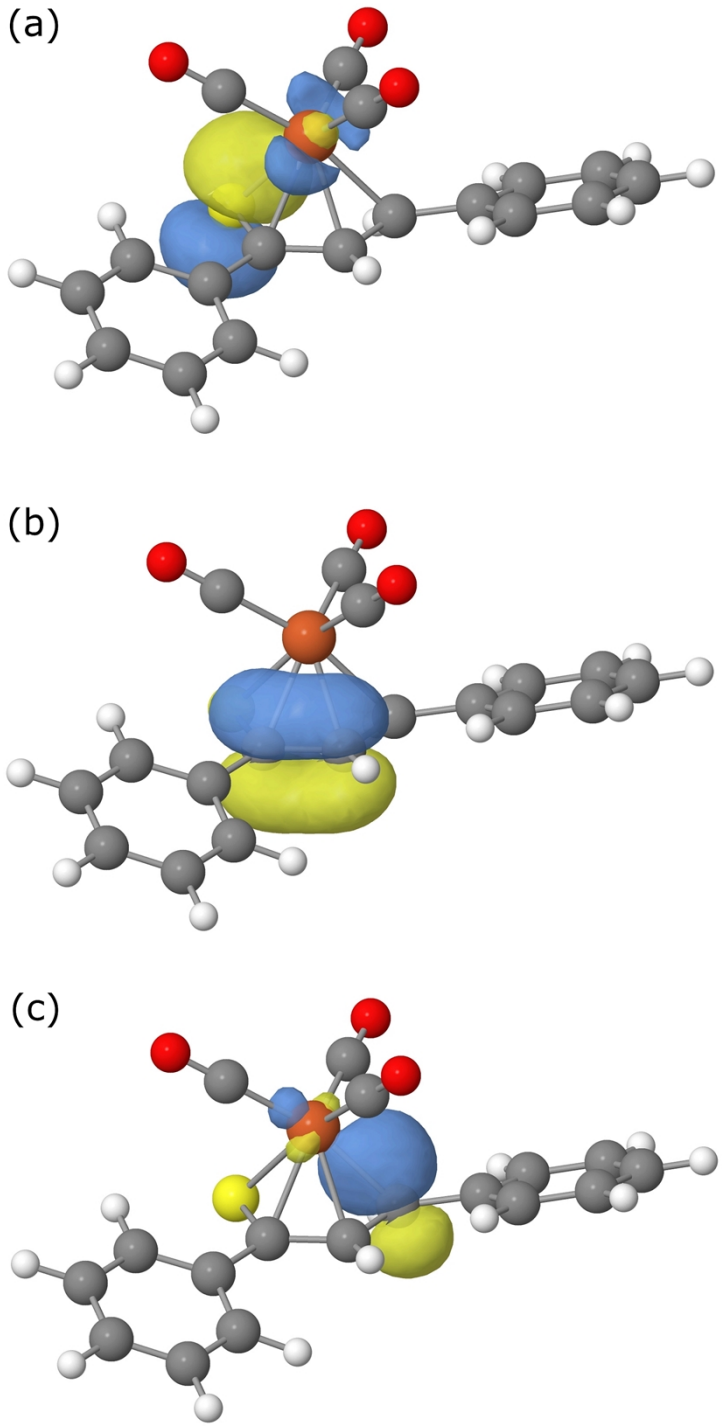

Figure S16. Contours of (a) σ-type Fe-S (b) π-type C^1-C^2 (c) σ-type Fe-C^3 NBO orbitals found for the optimal Lewis structure of complex **1**. The orbitals are plotted with an isovalue of 0.05 a.u. and their phases are marked in yellow and blue. Color codes for elements are explained in Figure 2.

Section S5. Cartesian coordinates for complexes 1–7 in their optimized geometries of the lowest energy

Complex **1**

C	2.963278	11.001159	7.436461
H	3.133273	10.500909	8.391814
C	3.182193	12.374411	7.345662
H	3.537706	12.922978	8.220521
C	2.936333	13.045945	6.150411
H	3.106641	14.122251	6.079014
C	2.455239	12.335190	5.050511
H	2.246605	12.853136	4.112024
C	2.231729	10.965664	5.142800
H	1.833643	10.414577	4.288753
C	2.500377	10.273256	6.331507
S	1.133792	7.964723	5.403477
C	2.278258	8.801320	6.427333
C	2.933192	8.014889	7.410764
H	3.725195	8.478980	8.003779
C	2.699887	6.616802	7.468511
H	1.674179	6.297971	7.258854
C	3.477336	5.689045	8.323257
C	4.674682	6.042429	8.963271
H	5.084329	7.049001	8.854253
C	5.366037	5.121140	9.745975
H	6.295331	5.420260	10.235608
C	4.879233	3.824326	9.903751
H	5.423943	3.102740	10.516041
C	3.691301	3.457621	9.272614
H	3.298579	2.445152	9.388696
C	3.000270	4.380575	8.493066
H	2.069640	4.086128	8.001044
Fe	3.346843	7.243721	5.539427
C	3.657533	8.139800	3.993580
C	3.060248	5.563694	4.965778
C	5.098248	7.132763	5.899299
O	3.813568	8.693339	3.011769
O	2.841524	4.496743	4.633748
O	6.213635	7.071861	6.122827

Complex **2**

S	1.302425	0.763975	6.263507
C	1.127062	-0.330817	7.579125
H	0.142933	-0.523004	8.002842
C	2.330054	-0.854890	7.961859
H	2.440419	-1.567372	8.779365
C	3.413292	-0.365147	7.177164
H	4.454413	-0.659117	7.316134
C	3.022468	0.526849	6.207472
C	2.537525	3.967608	2.073165
H	1.801334	3.228541	2.398935
C	2.137471	5.004827	1.236700
H	1.092087	5.079642	0.929883
C	3.070579	5.936186	0.780026
H	2.757644	6.748480	0.120673
C	4.404804	5.817032	1.162388
H	5.143563	6.537804	0.805684
C	4.805606	4.777628	1.999657
H	5.852584	4.679959	2.293200
C	3.876389	3.845352	2.472336
S	5.909911	2.047871	3.304199
C	4.311274	2.751991	3.387319
C	3.469448	2.276236	4.425264
H	2.447180	2.661937	4.494751
C	3.897514	1.193699	5.237419
H	4.958253	1.177984	5.506381
Fe	3.989769	0.722636	3.159375
C	4.215613	0.794678	1.357228
C	2.292722	0.174009	2.988705
C	4.759025	-0.843924	3.598620
O	4.392719	0.856501	0.236129
O	1.215650	-0.169065	2.847982
O	5.264567	-1.813689	3.915116

Complex **3**

S	-6.459731	-8.662116	-16.050204
C	-5.849670	-7.047248	-15.772805
C	-5.832110	-6.596476	-14.427137
H	-5.393319	-5.617740	-14.209668
C	-6.202304	-7.484008	-13.383980
H	-7.031337	-8.162039	-13.608654
C	-6.020721	-7.177880	-11.945671
C	-6.644847	-8.008265	-11.002691
H	-7.254119	-8.845762	-11.352367
C	-6.498442	-7.783680	-9.636981
H	-6.994365	-8.445071	-8.923249
C	-5.722789	-6.718186	-9.181870
H	-5.605677	-6.539256	-8.111099
C	-5.097472	-5.882812	-10.106344
H	-4.487803	-5.044632	-9.762083
C	-5.242547	-6.110845	-11.472460
H	-4.735415	-5.442379	-12.171692
S	-4.813880	-4.584157	-16.640983
C	-5.426004	-6.191451	-16.893088
C	-5.421953	-6.504970	-18.229756
H	-5.771492	-7.469909	-18.596428
C	-4.920886	-5.453810	-19.048582
H	-4.840964	-5.511332	-20.133983
C	-4.552618	-4.354518	-18.323740
H	-4.148197	-3.412051	-18.689411
Fe	-4.660678	-8.291736	-14.605946
C	-3.307116	-7.536701	-13.708306
C	-4.790753	-9.831673	-13.684593
C	-3.586543	-8.735086	-16.003990
O	-2.441395	-7.051940	-13.148766
O	-4.920554	-10.798033	-13.096771
O	-2.953999	-9.021939	-16.904203

Complex **4**

Fe	3.976158	4.175781	11.440072
S	2.917023	3.718924	7.577243
C	3.488448	5.084922	8.506383
C	4.355025	5.989362	7.843777
C	4.640670	5.806427	6.465078
C	5.369774	6.798404	5.640485
C	5.824154	6.407589	4.371851
C	6.503059	7.296996	3.544147
C	6.745332	8.602864	3.968570
C	6.301357	9.006627	5.226898
C	5.619858	8.115937	6.052572
C	3.140195	5.257196	9.927878
C	3.787986	6.128364	10.865386
C	3.176692	5.940554	12.135907
C	2.153083	4.959796	11.994099
C	2.127608	4.536980	10.637484
C	5.749208	3.362309	10.812560
C	4.709355	2.389816	10.748674
C	4.177683	2.227875	12.060428
C	4.888991	3.099316	12.936125
C	5.860418	3.800868	12.164382
H	6.846043	6.967534	2.560953
H	4.661653	6.894061	8.374761
H	5.278960	8.463784	7.030123
H	7.277439	9.303373	3.321682
H	1.481633	3.778667	10.200217
H	4.356240	1.893092	9.846500
H	4.752943	4.768210	6.137752
H	6.484833	10.026986	5.570537
H	5.637241	5.385486	4.032308
H	1.517285	4.579449	12.791028
H	6.332454	3.726533	9.968434
H	6.549632	4.556130	12.537663
H	3.462239	6.440365	13.059445
H	4.626696	6.790459	10.659415
H	4.706509	3.224413	14.001820
H	3.353322	1.574201	12.339168
Fe	2.552301	5.905553	6.836911
C	0.900158	5.771051	7.578205
C	2.262296	5.506128	5.107356
C	2.441674	7.689143	6.738231
O	-0.128867	5.641767	8.045811
O	2.119870	5.225209	4.012948
O	2.363964	8.824798	6.686131

Complex **5**

Fe	-0.563036	12.129983	1.668342
S	1.901784	10.577421	4.458625
C	0.981790	9.878115	3.146042
C	1.586927	8.805045	2.449690
C	2.837271	8.295616	2.897144
C	3.282266	5.150980	1.293646
H	2.735699	4.371279	0.771545
C	4.588411	5.307097	1.639657
H	5.399184	4.612545	1.434784
C	3.398005	7.073038	2.332573
C	4.666701	6.563577	2.321392
H	5.547361	7.035140	2.750018
O	2.557416	6.213025	1.708141
C	-0.327687	10.416493	2.739174
C	-1.115384	11.356231	3.477654
C	-2.274111	11.659182	2.711812
C	-2.213597	10.914137	1.498429
C	-1.016544	10.145123	1.510343
C	1.321174	12.878410	1.375359
C	0.702263	12.593535	0.123447
C	-0.491837	13.368840	0.035426
C	-0.608866	14.133662	1.233015
C	0.511579	13.829586	2.061282
H	2.229634	12.419140	1.762544
H	-0.843245	11.772337	4.445222
H	1.019555	8.275086	1.680485
H	-2.942819	10.943223	0.691195
H	-1.421306	14.814341	1.480364
H	-0.674971	9.492780	0.709232
H	3.579484	9.016744	3.249570
H	0.703236	14.229231	3.055189
H	1.066355	11.891366	-0.624275
H	-3.059004	12.357685	2.994624
H	-1.197831	13.365191	-0.792927
Fe	1.384208	8.297054	4.441188
C	0.680605	6.697426	4.031982
C	2.648422	7.768483	5.606207
C	-0.015775	8.710666	5.520952
O	0.210445	5.688963	3.790826
O	3.479009	7.460041	6.321714
O	-0.873467	9.011884	6.204968

Complex **6**

Fe	-0.590652	7.046830	1.760866
S	2.026487	8.632246	4.430134
C	0.994269	9.308229	3.190943
C	1.518479	10.401606	2.458746
H	0.875743	10.902624	1.728464
C	2.779055	10.948522	2.817963
H	3.582881	15.224926	0.416619
C	3.315671	12.178317	2.224559
C	4.595044	12.659902	2.365852
H	5.353358	12.141440	2.953920
C	4.814597	13.887629	1.677570
H	5.764060	14.423022	1.670227
C	3.699460	14.326678	1.020386
S	2.374517	13.249305	1.231836
C	-0.323977	8.731151	2.875574
C	-1.006458	7.735484	3.643610
H	-0.630063	7.294982	4.564416
C	-2.216617	7.412068	2.972744
H	-2.944127	6.669843	3.294918
C	-2.293774	8.200939	1.788747
H	-3.089411	8.168250	1.047012
C	-1.130108	9.016355	1.723725
H	-0.886797	9.706575	0.918375
C	0.990604	6.717335	0.497214
H	1.657800	7.491595	0.122249
C	-0.224745	6.287485	-0.111800
H	-0.647856	6.672586	-1.037779
C	-0.803994	5.286172	0.720529
H	-1.746635	4.772290	0.541654
C	0.053134	5.098083	1.843884
H	-0.122412	4.419523	2.676482
C	1.161623	5.982112	1.706086
H	1.974608	6.108085	2.419393
H	3.545815	10.235611	3.136690
Fe	1.431678	10.892165	4.466062
C	0.633580	12.462786	4.134899
C	2.766947	11.468803	5.524795
C	0.139027	10.417328	5.649434
O	0.103595	13.452791	3.945538
O	3.644180	11.811142	6.165302
O	-0.649431	10.078881	6.396261

Complex **7**

S	1.133840	8.009214	5.365417
C	2.324117	8.788082	6.377192
C	2.958244	7.978704	7.352207
H	3.766524	8.418785	7.948222
C	2.708436	6.581712	7.384470
H	1.670978	6.281601	7.202476
C	3.504849	5.670989	8.281649
H	3.046359	5.619764	9.282836
H	3.529977	4.645614	7.885212
H	4.544130	6.010461	8.406282
C	2.587374	10.264903	6.284325
H	2.558542	10.605669	5.240929
H	1.804887	10.813618	6.831383
H	3.561226	10.526835	6.724520
Fe	3.335862	7.224030	5.469412
C	2.990442	5.568202	4.870897
C	5.077202	7.055734	5.824356
C	3.642395	8.165304	3.951123
O	2.738989	4.513257	4.520640
O	6.186851	6.951635	6.068940
O	3.794933	8.763886	2.994578

References

1. Nonius B.V., *COLLECT Data collection software*, Delft, The Netherlands, 1998.
2. Z. Otwinowski and W. Minor, in *Methods in Enzymology, vol. 276, Macromolecular Crystallography, Part A*, eds. C. W. Carter and R. M. Sweet, Academic Press, New York, USA, 1997, pp. 307–326.
3. L. Krause, R. Herbst-Irmer, G. M. Sheldrick and D. Stalke, *J. Appl. Cryst.*, 2015, **48**, 3−10.
4. G. M. Sheldrick, *Acta Cryst. A*, 2015, **71**, 3−8.
5. G. M. Sheldrick, *Acta Crystallogr. C*, 2015, **71**, 3−8.
6. D. Kratzert and I. Krossing, *J. Appl. Cryst.*, 2018, **51**, 928–934.
7. Siemens Analytical X-ray Instruments Inc., *XP*, Karlsruhe, Germany, 1990.
8. S. J. Gravelle, L. J. van de Burgt and E. Weitz, *J. Phys. Chem.*, 1993, **97**, 5272.
9. T. Leitner, I. Josefsson, T. Mazza, P. S. Miedema, H. Schröder, M. Beye, K. Kunnus, S. Schreck, S. Düsterer, A. Föhlisch, M. Meyer, M. Odelius and P. Wernet, *J. Chem. Phys.*, 2018, **149**, 044307.
10. M. Poliakoff, *J. Chem. Soc. Dalton Trans.*, 1974, **1974**, 210–212.
11. M. Zhou and L. Andrews, *J. Chem. Phys.*, 1999, **110**, 10370−10379.
12. J. K. Burdett, *J. Chem. Soc. Faraday Trans. 2*, 1974, **70**, 1599−1613.
13. L. A. Barnes, M. Rosi and C. W. J. Bauschlicher, *J. Chem. Phys.*, 1991, **94**, 2031–2039.
14. M. Elian and R. Hoffmann, *Inorg. Chem.*, 1975, **14**, 1059–1076.
15. G. Frenking, I. Fernández, N. Holzmann, S. Pan, I. Krossing and M. Zhou, *JACS Au*, 2021, **1**, 623−645.
16. S. F. Boys and F. Bernardi, *Mol. Phys.*, 1970, **19**, 553–566.
17. F. Weinhold and C. R. Landis, *Valency and bonding: a natural bond orbital donor–acceptor perspective*, Cambridge University Press, New York, 2005.